Sedimentology (2005) **52**, 339–361 doi: 10.1111/j.1365-3091.2005.00701.x

Characterization, lateral variability and lateral extent of discontinuity surfaces on a Carbonate Platform (Barremian to Lower Aptian, Oman)

UTE SATTLER*,[1], ADRIAN IMMENHAUSER*, HEIKO HILLGÄRTNER† and MATEU ESTEBAN‡
**Faculty of Earth and Life Sciences, Vrije Universiteit Amsterdam, De Boelelaan 1085, 1081 HV Amsterdam, The Netherlands (E-mail: ute.sattler@falw.vu.nl)*
†Shell International E&P BV, Volmerlaan 8, Postbus 60, 2280 AB Rijswijk, The Netherlands
‡Carbonates Int. Iberia SL, Carrer Sant Jaume 11, E-07314 Caimari, Mallorca, Spain

ABSTRACT

Hiati of various duration in carbonates are commonly expressed as discontinuity surfaces. The understanding of processes that form and affect these surfaces leads to an improved sequence-stratigraphic interpretation, a reliable outcrop correlation, and better models for reservoir compartmentalization. Various intraformational discontinuities were analysed and interpreted in a well-exposed study window, 2·5 km in lateral length and 60 m in height comprising the Barremian-Aptian Qishn Formation (Haushi-Huqf area, central Oman). This study focuses on the lateral extent and morphology of the surfaces, the petrography of the underlying rocks, and the facies changes and geochemical trends across these discontinuities. Furthermore, the lateral variability of discontinuity surfaces was documented. Three genetic types of discontinuities are differentiated: (i) erosion surfaces; (ii) omission surfaces (hard- and firmgrounds); and (iii) composite surfaces with evidence for both subaerial exposure and submarine boring. Field observations, combined with petrographic and geochemical data, suggest that 17 surfaces are laterally extensive for at least 20 km and record relative sea-level fluctuations of regional scale. In contrast, a large number of laterally limited surfaces (<1 km) are related to locally active processes such as waves and current erosion. The lateral variability along extensive surfaces is the result of the depositional environment below the discontinuity, the sea-floor topography, waves and currents and differential erosion. The most pronounced lateral variability is present along six laterally extensive composite surfaces that record terrestrial exposure and subsequent flooding of a tidal flat environment. This variability is caused by spatial variability in the tidal flat environment, meteoric alteration and differential erosion. This study emphasizes the spatial and temporal complexity of processes that form and modify discontinuity surfaces. This variability must be kept in mind when interpretations and correlations are based on one-dimensional sections or cores.

Keywords Carbonate platform, Cretaceous, discontinuity surface, Oman, subaerial exposure.

INTRODUCTION

Discontinuity surfaces are surfaces in the sedimentary record related to breaks in sedimentation (Clari *et al.*, 1995). In the Oman study area, this includes omission surfaces (hardgrounds and

[1]Present address: OMV E+P, Gerasdorfer Strasse 151, A-1210 Vienna, Austria (E-mail: ute.sattler@omv.com).

firmgrounds), erosion surfaces and composite surfaces that are penetrated by meteoric features and borings. Heim (1924) first introduced the term 'discontinuity surfaces', which was later defined by Bromley (1975) as sedimentary breaks which are 'more minor in rank than disconformities'. These surfaces are used as marker horizons for the correlation of stratigraphic sections (e.g. Kauffman *et al.*, 1991; Immenhauser *et al.*, 2000), and as boundaries for depositional units in sequence stratigraphy (e.g. Mitchum *et al.*, 1977; Sarg, 1988; Handford & Loucks, 1993 and references therein). Furthermore, flow barriers or flow conduits in petroleum reservoirs can develop beneath discontinuity surfaces (Read & Horbury, 1994; Cander, 1995; Wagner *et al.*, 1995). Numerous authors have studied discontinuity surfaces (e.g. Heim, 1924; Shinn, 1969; Bromley, 1975; Marshall & Ashton, 1980; Riding & Wright, 1981; Allan & Matthews, 1982; Wright, 1994; Clari *et al.*, 1995; Fouke *et al.*, 1995; Hillgärtner, 1998; Immenhauser *et al.*, 2000; Wilson & Taylor, 2001; Immenhauser & Scott, 2002), but little research has yet been done to demonstrate how characteristic features such as surface morphology, petrography and facies change across a discontinuity and geochemistry changes spatially along the surface (lateral variability). Ignoring the lateral variability of a discontinuity surface can result in poor correlations of spatially separated sections and misinterpretations in sequence stratigraphy (Kauffman *et al.*, 1991). The impact a given discontinuity surface can have on reservoir compartmentalization strongly depends on its lateral extent and lateral variability and on the associated diagenesis of underlying rocks.

The purpose of this study was to describe and interpret discontinuity surfaces and the underlying altered rock interval in terms of lateral extent and morphology, petrography, geochemistry, facies change across the surface, and to assess their lateral variability. Furthermore, the temporal succession of processes that generate and alter discontinuity surfaces and the underlying strata is investigated.

The exceptionally well-exposed Barremian to Lower Aptian Qishn Formation (corresponds to the Shu'aiba and Kharaib Formations of Le Metour *et al.*, 1995 and Immenhauser *et al.*, 2004) at the Haushi-Huqf High of Oman (referred to as 'Huqf') provides an ideal study area, where numerous discontinuities can be laterally traced and correlated across distances of up to 21 km. The Qishn Formation is capped by a regionally important unconformity (top-Qishn unconformity) that represents a hiatus of about 8 Myr duration or more. The focus of this study, however, are smaller scale, intraformational discontinuity surfaces of the Qishn. These are compared and correlated with the same stratigraphic interval (the Shu'aiba Formation) at Jabal Madar, 170 km further to the north (Fig. 1).

GEOLOGIC SETTING

Stratigraphic and geotectonic setting

Beydoun (1964) defined the Upper Barremian to Lower Aptian Qishn Formation in South Yemen. The Qishn Formation of the Huqf area corresponds to the (Lower) Shu'aiba and (Upper) Kharaib Formations (including Hawar member) at Jabal Madar, northern Oman (Immenhauser *et al.*, 2004; Fig. 2). These formations are a major hydrocarbon reservoir in the subsurface of the Middle East and have therefore been the subject of many previous studies (refer to Alsharan & Nairn, 1997 or Hughes, 2000 for an overview). Except for two studies (Montenat *et al.*, 2003; Immenhauser *et al.*, 2004), no research has focused on the corresponding stratigraphic interval in the Huqf area. There, the Qishn Formation onlaps an approximately NE–SW trending structural high, the 'Haushi-Huqf High' (*sensu* Ries & Shackleton, 1990; Fig. 1A). The Barremian–Aptian depositional environment of the Qishn Formation was a wide, locally restricted carbonate platform covering the proximal shoulder of the Haushi-Huqf High (Immenhauser *et al.*, 2004). To the north and west, the platform grades into the deep shelf facies of the interior Oman Shu'aiba basins that are connected northwards via the Bab Basin (Van Buchem *et al.*, 2002) to the Tethyan Sea (Fig. 1B). Local structural highs, such as saltdomes, complicate the overall basin geometry (Immenhauser *et al.*, 2004). The Qishn Formation equivalent (Kharaib and Shu'aiba Formations) at Jabal Madar, 170 km north of the Huqf, is exposed due to salt doming. The Kharaib and Shu'aiba Formations at Jabal Madar are comprised of shallow-marine carbonates that were deposited in closer vicinity to the Bab Basin than the Qishn deposits (Fig. 1B). Therefore, the facies succession at Jabal Madar is bathymetrically comparable with that in the Huqf area, but the environment is less restricted.

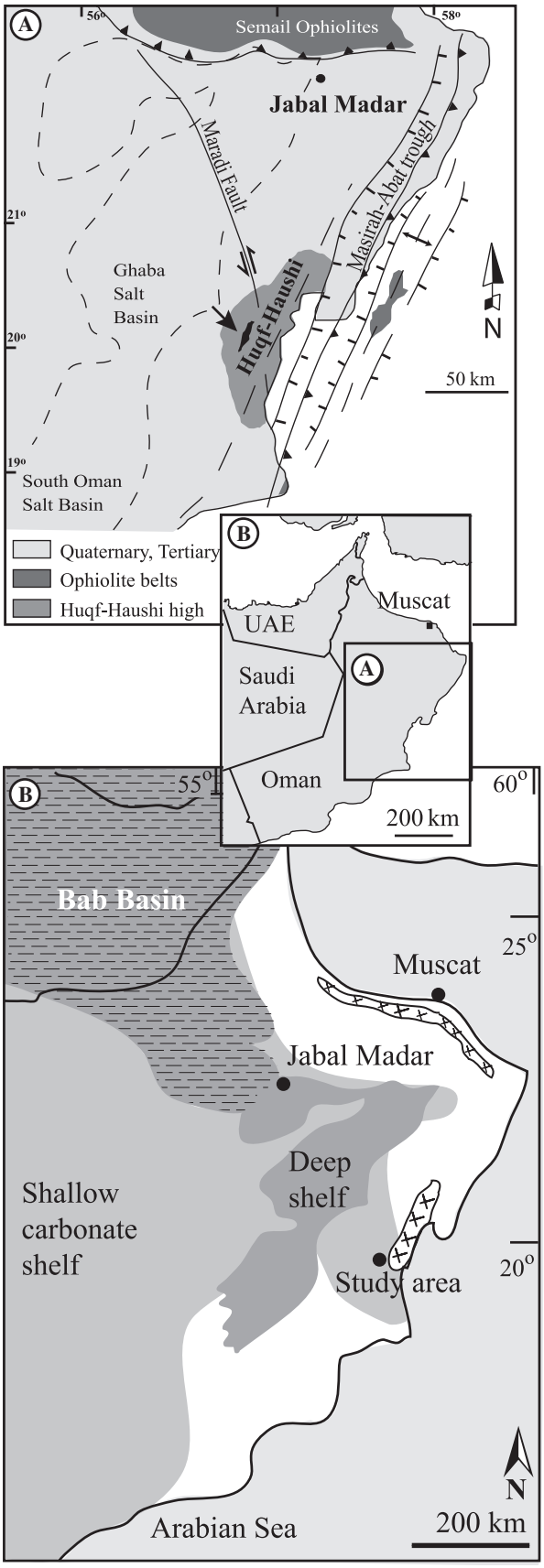

Fig. 1. (A) Geotectonic map of eastern Oman showing the main structural elements the Huqf study area (arrow) and Jabal Madar (modified after Loosveld *et al.*, 1996 and Immenhauser *et al.*, 2004). (B) Aptian palinspastic reconstruction of the eastern portions of the Arabian Peninsula. The deeper shelf facies of the Shu'aiba Basin and the Bab Intrashelf Basin are superimposed on the shallow marine carbonate shelf (modified after Hughes, 2000).

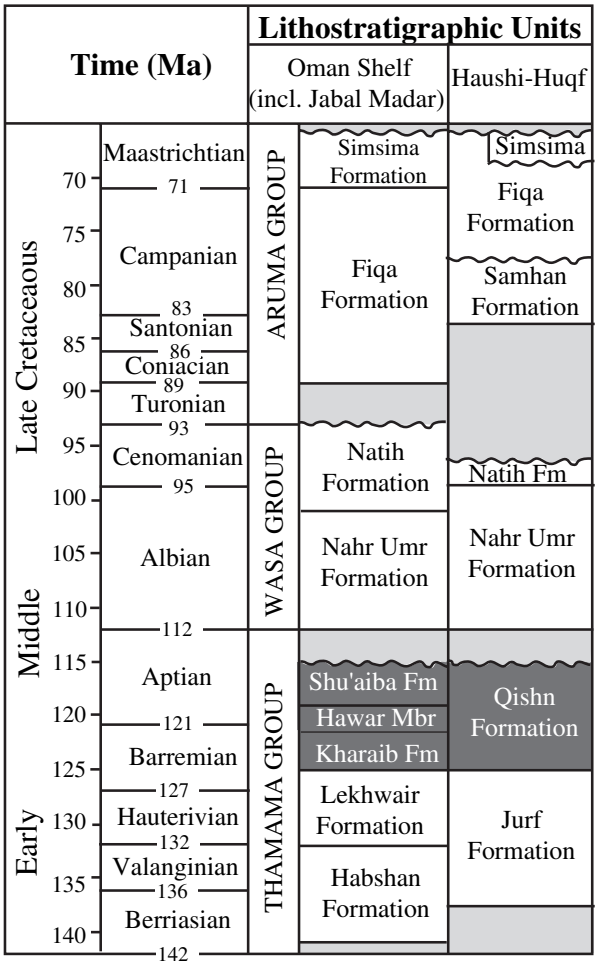

Fig. 2. Cretaceous chronostratigraphy of Oman. The Qishn Formation in the Huqf area corresponds with the Kharaib (including the Hawar member) and part of the Shu'aiba Formations (marked in dark grey) of northern Oman (modified after Immenhauser *et al.*, 2004). Unconformities denoted in light grey.

Sequence stratigraphic setting

Figure 3 provides an overview of the main depositional environments differentiated in the Qishn Formation. Three major depositional sequences were identified (Sequences II to IV on Fig. 4; Immenhauser *et al.*, 2004) that are deposited onto

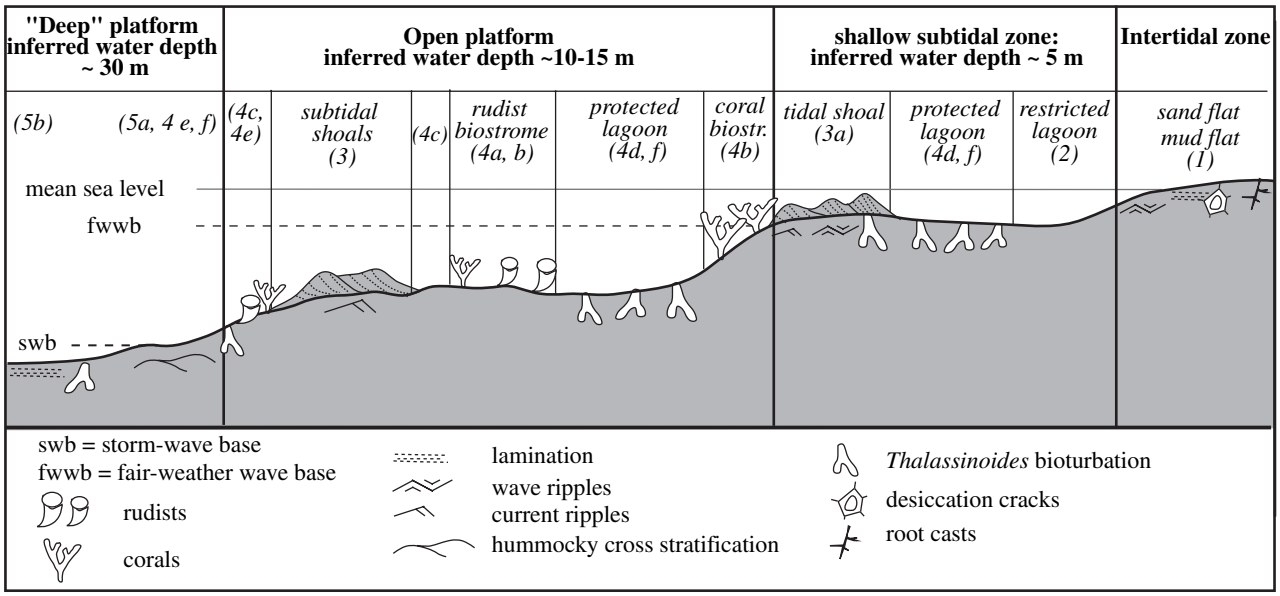

Fig. 3. Overview of palaeodepositional environment recorded in the Qishn Formation of the Huqf area. Numbers relate to facies classification given in Fig. 5 (modified after Immenhauser *et al.*, 2004).

the Jurf Formation (Sequence I, Fig. 4 this study and Immenhauser *et al.*, 2004). Sequence I is comprised of a succession of dolomitized tidal flat deposits. Sequence II is characterized by shallow-marine, high-energy shoal deposits at the base followed upsection by marly, deeper platform sedimentary rocks and tidal flat deposits. Lithosomes with *in situ* rudists were found locally. High-energy shoals and tidal flat deposits dominate Sequence III (Fig. 4). Sequence IV forms the upper portions of the Qishn Formation. It commences with tidal flat deposits that gradually deepen into open lagoonal deposits at the base of the sequence. The upper part of Sequence IV is mainly composed of high-energy grainstones with reworked *Lithocodium*/*Bacinella* oncoids. The top-Qishn unconformity, capping Sequence IV, is not preserved in the studied outcrops, but exposed a few kilometres to the north. The top-Qishn unconformity is indicated in the 'AP8 sequence' of the sequence stratigraphic framework of the Arabian Plate by Sharland *et al.* (2001). Further correlation with Sharland *et al.* (2001) is problematic because Sharland *et al.* (2001) use maximum flooding surfaces for correlation whereas present work is based on exposure surfaces, and has significantly higher spatial and temporal resolution. For more detail on sequence stratigraphy and regional sedimentology of the Huqf area see Immenhauser *et al.* (2004).

METHODOLOGY AND TERMINOLOGY

Field observations

In the Huqf area, a 2·5 km wide and 60 m high study window, oriented approximately parallel to the Haushi-Huqf High and to the strike of palaeofacies belts, was selected. Here, discontinuity surfaces were physically traced on the outcrop between seven closely spaced sections. The morphology, petrographic characteristics and facies contrasts of these surfaces and how these features change spatially was evaluated. Discontinuity surfaces were classified according to their lateral extent. Discontinuity surfaces laterally extending throughout the study window were correlated with Section S018 located 19 km southwards as calculated from a topographic map (Fig. 4). In this study, these regional surfaces are referred to as 'laterally extensive' discontinuities. In contrast, surfaces with an extent >100 m and <1 km are referred to as 'laterally limited'. Additionally, 30 small-scale discontinuities with a lateral extent <100 m were analysed and termed 'laterally limited'. Discontinuity surfaces observed in the Huqf area were compared with those of the same stratigraphic interval at Jabal Madar in northern Oman. A correlation of Jabal Madar with the Huqf is based on facies architecture, tidal-flat marker intervals and discontinuity surfaces (Fig. 5).

The key to abbreviations used for discontinuity surfaces in the Huqf area (CS 1–6, ES 1–8, OS 1 and SE 1, 2) is given in Figs 4 and 5, where their stratigraphic position is also indicated. Abbreviations used for discontinuity surfaces at Jabal Madar (Ds A-I) are explained in Fig. 5.

Petrographic and geochemical studies

A total of 395 thin sections, collected from around stratigraphic hiati, were studied using standard light and cathodoluminescence microscopy for microfacies and diagenetic overprint.

Bulk-micrite (263) and cement samples (71) were analysed on a Finnigan 252 mass spectrometer equipped with an automated carbonate extraction line. Carbonate-cement powder samples were obtained using a dental drill, or a MicroMill™ Sampler. Samples (20 to 50 μg) were dissolved in concentrated orthophosphoric acid at a temperature of 80°C. Repeated analyses of carbonate standards show a reproducibility of 0·08‰ for $\delta^{18}O$ and 0·05‰ for $\delta^{13}C$. All results are presented as parts per thousand relative to the VPDB standard.

CHARACTERIZATION, LATERAL EXTENT AND VARIABILITY OF DISCONTINUITY SURFACES

Seventeen laterally extensive and 13 laterally limited discontinuities are recognized within the Qishn in the study area (Fig. 4). Additionally, 30 discontinuity surfaces of <100 m lateral extent were analysed. From a genetic point of view, three types of surfaces are differentiated: (i) composite surfaces; (ii) omission surfaces; and (iii) erosion surfaces.

Composite surfaces

The descriptive term 'composite surface' is used here for six laterally extensive discontinuity surfaces that record meteoric features (see *Discussion*) and marine borings (CS 1–CS 6, Fig. 4). Immenhauser *et al*. (2004) traced composite surfaces for 100 km in the Qishn Formation of the Huqf area. Four of the composite surfaces correspond to discontinuities at Jabal Madar, 170 km north of the Huqf area (Fig. 5).

Tidal flat deposits underlying composite surfaces

Tidal flat deposits of the Qishn Formation are laminated mudstones and wackestones that were accumulated on a mud flat, or fine-grained packstones and grainstones of a sand flat environment. Peloids and milioliid foraminifera are the main components in packstones and grainstones that also contain smaller amounts of shell debris and sponge spiculae. Three kinds of sediment reworking are present: (i) diffuse mixing of different sediment layers, resulting in a patchy texture (Fig. 6A); (ii) *in situ* brecciation of sediment layers below composite surfaces and channels (Fig. 6B); and (iii) subvertical and horizontal cracking of beds (Fig. 6A). Shallow, symmetric tidal channels (Fig. 6C) have diameters ranging from <1 m to 15 m. Massive mudstones and wackestones with bird's-eyes and circumgranular cracks usually infill the channels.

Circumgranular cracks and bird's-eye structures are common in the tidal facies. Crystal silts geopetally infill a number of vugs, mouldic pores and thin tubes (up to 5 mm in diameter) that penetrate tidal flat deposits with varying density. These tubes show downward bifurcation and are filled with non-luminescent, blocky calcite of orange, yellow or transparent color (Fig. 7A). Darker sedimentary rock concentrically surrounds some tubes. This sedimentary rock contains alveolar textures (Esteban, 1974) below one discontinuity (Fig. 7B and C). Several centimetres to 1 dm thick voids are common in the tidal flats. Thinner voids tend to surround and penetrate larger ones. The diameter of voids decreases downward from the composite surfaces and bedding planes (Fig. 7D,E and F). *In situ* brecciation commonly accompanies the voids. These tubes and voids are more abundant in channel-fillings than they are on supratidal flats, where polygonal mudcracks (Fig. 7G) and tepees (Fig. 7H) are locally abundant.

Tidal flat deposits of the Huqf are interpreted as closely spaced subenvironments with channels, mudflats and sandflats. Milioliid-dominated fauna as observed in the Huqf, are characteristic for restricted or even hypersaline environments (Geel, 2000). Different subenvironments result in different types of sediment reworking: (i) burrowing in soft, unconsolidated sediment in sub to intertidal settings produces diffuse structures of mixed sediment; (ii) desiccation on supratidal flats results in polygonal mudcracks and in horizontal and subvertical cracks locally reworked into *in situ* breccias during subsequent flooding. Similar processes have been described from modern supratidal settings (Kendall & Warren, 1987).

Vugs and mouldic pores, filled with crystal silt, are common in vadose conditions (vadose silts

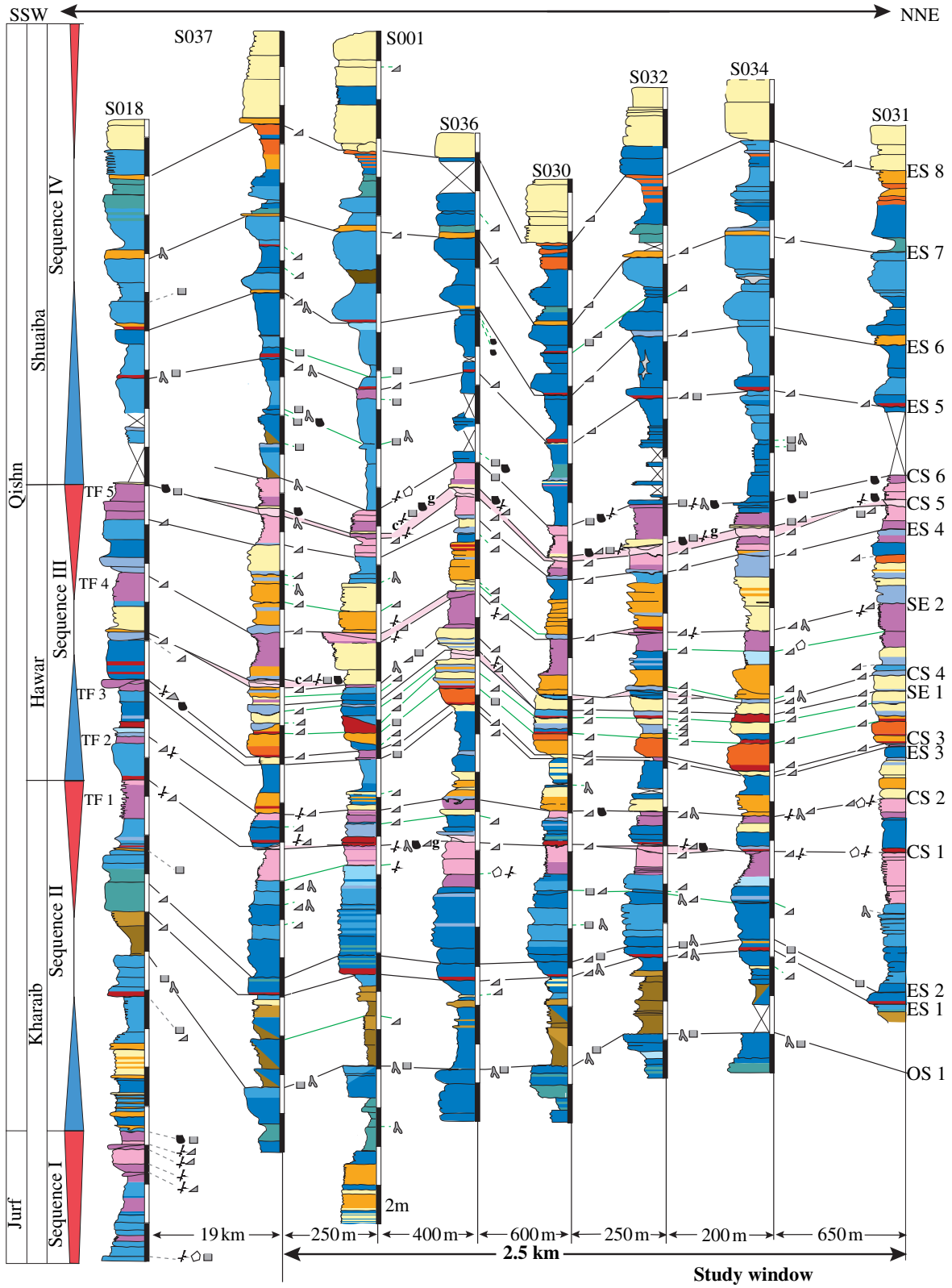

Fig. 4. Sections measured in the Huqf area. Overview of the spatial and temporal distribution and nature of discontinuity surfaces. Petrographic features indicating interruptions in sedimentation are indicated to the right of each section. Sequence stratigraphic framework is based on Immenhauser *et al.* (2004). OS, omission surface; ES, erosion surface; CS, composite surface; SE, discontinuity related to subaerial exposure; TF, tidal flat interval. For key to symbols and color code, refer to Fig. 5.

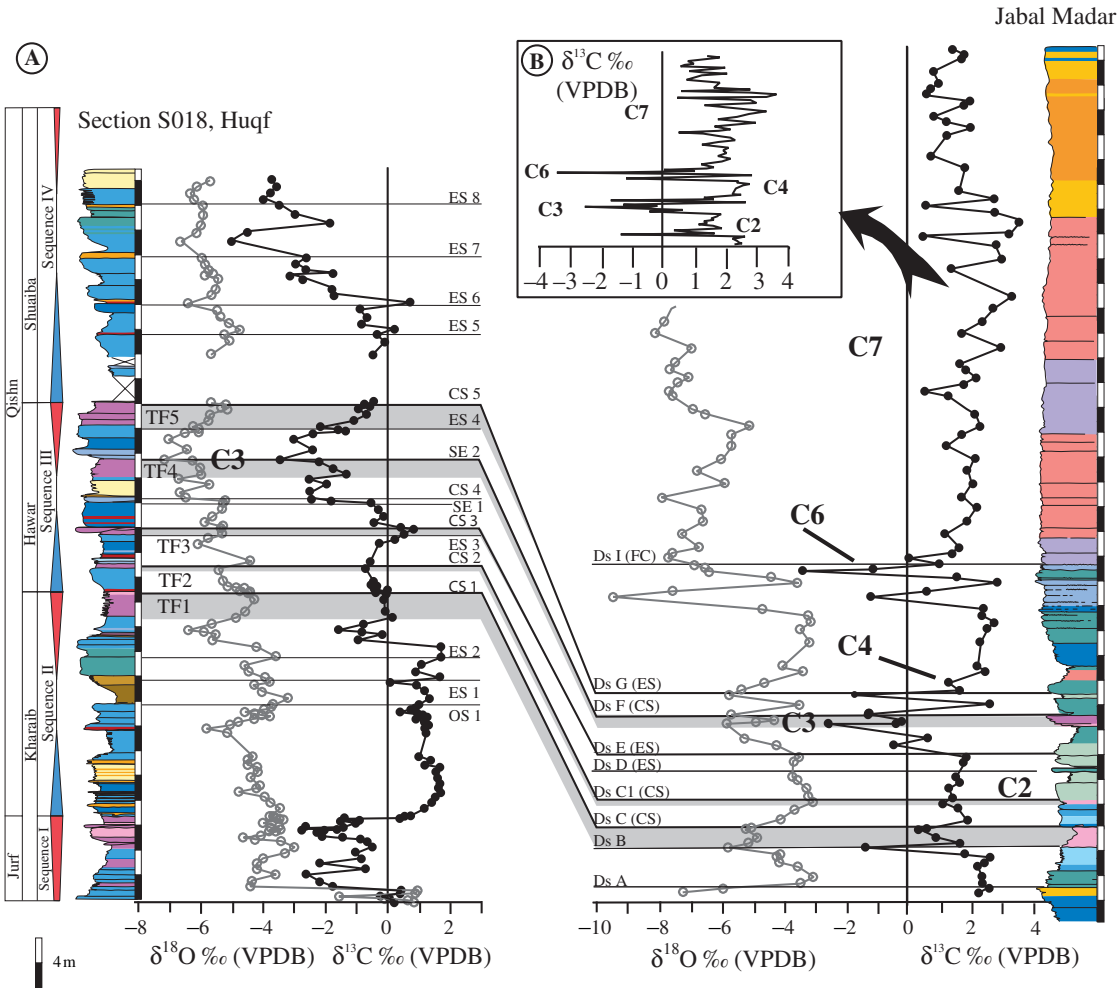

Facies classification and interpretation

1. Intertidal zone
- Mudflat — 1a
- Sand flat — 1b

2. Restricted platform (lagoon)
- Poor/restricted fauna — 2a
- Argillaceous restricted fauna — 2b

3. High-energy platform (x-bedded)
- Shoals — 3a
- *Lithocodium-Bacinella* oncoid facies — 3b
- Rudist facies — 3c

4. Open platform (lagoon)
- Rudist biostromes — 4a
- Coral lagoon — 4b
- Oyster facies — 4c
- Protected diverse fauna facies — 4d
- Diverse fauna facies — 4e
- Orbitolinid-dominated facies — 4f
- Orbitolinid-dominated facies (low energy) — 4g
- Bioconstructed *Lithocodium/Bacinella* facies — 4h

5. Deep platform (argillaceous lagoon)
- Storm influenced facies — 5a
- Muddy facies — 5b

Discontinuity surfaces

lateral extent: unknown
lateral extent: <100 m
lateral extent: > 100 m< 1 km
lateral extent: at least 21 km

CS	composite surface
ES	erosion surface
OS	omission surface
SE	subaerial exposure surface
Ds	discontinuity surface

Key to symbols

roots
boring
erosion
impregnation
abundant *Thalassinoides*
g glaebules
c epikarst
TF tidal flat interval

Fig. 5. (A) Lithostratigraphy and chemostratigraphy of Section S018 in the Huqf section and Jabal Madar. Correlation of the sections is based on the facies architecture, tidal-flat marker intervals (highlighted in pink) and discontinuity surfaces. Numbers C2 to C7 refer to segments of the Tethyan δ^{13}C-curve (Menegatti *et al.*, 1998). The OAE1a is contained in segments C4 through C7. (B) δ^{13}C curve of Jabal Madar re-scaled with respect to the *y*-axes to highlight δ^{13}C-trends.

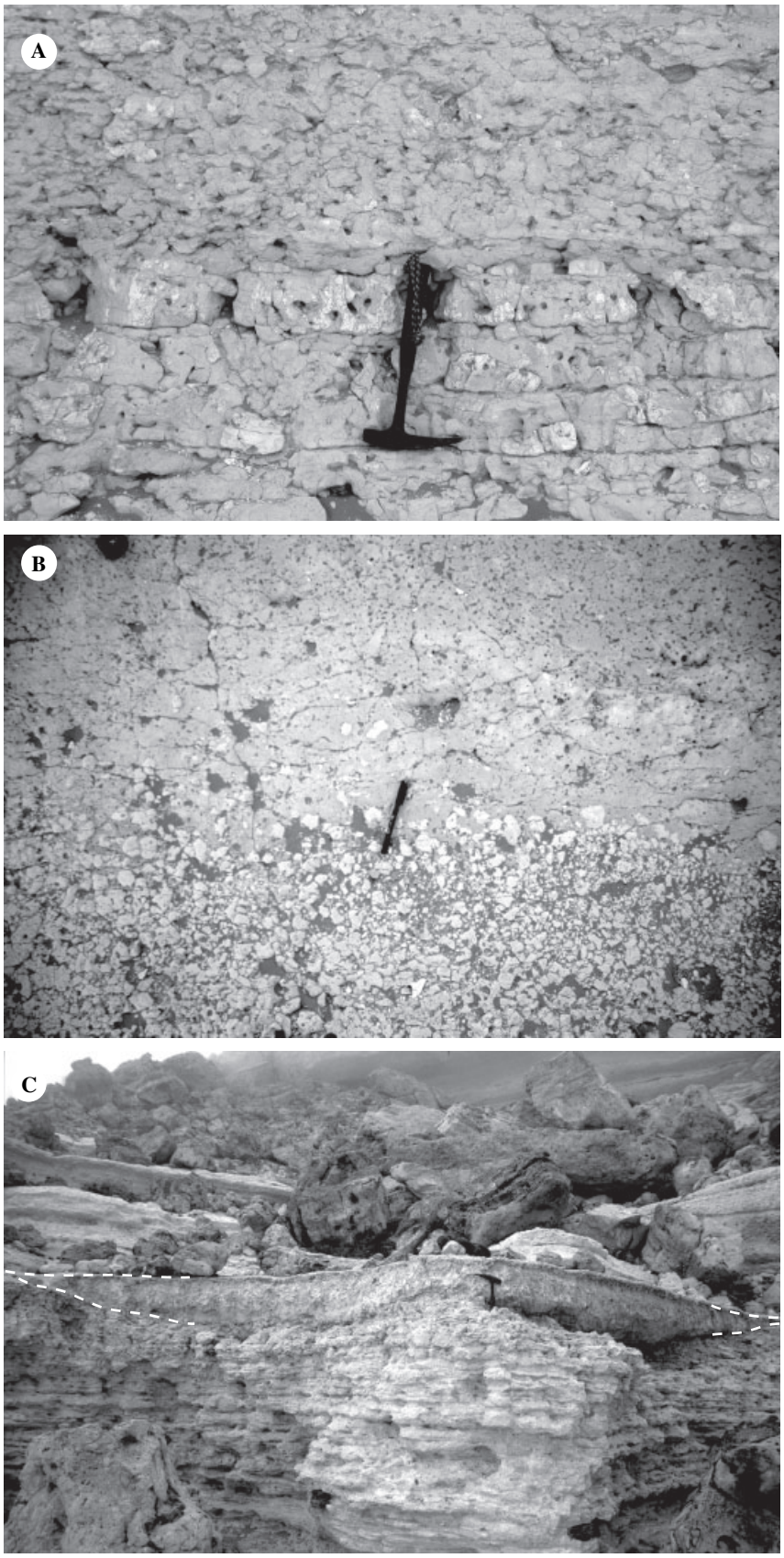

Fig. 6. Tidal flat environment. (A) Upper part: diffuse mixing of different sediment layers caused by bioturbation of unconsolidated sediment. Lower part: subvertically and horizontally cracked beds caused by desiccation of consolidated sediment (section view). (B) *In situ* brecciated or slightly transported limestones, pointing to early lithification, desiccation and reworking on a tidal flat (section view). (C) Symmetric, tidal channel (marked by white, dashed line) cutting into thinly bedded, laminated supratidal mudstones.

sensu Dunham, 1969). Downward-bifurcating thin tubes point to root activity in the terrestrial or tidal flat environment (Klappa, 1980). Thick voids surrounded by thinner voids have been interpreted as enlarged, hierarchic root systems comparable with Freytet & Plaziat's (1982) *pedogenetic pseudo-microkarst*. Alternations of desiccation, rain, flooding and storms rework sediment, enlarge root casts and fill them with high-energy sediment. Several pulses of flooding and storm activity alternate with several periods of plant colonization in Freytet & Plaziat's (1982) model. Similarly in the Huqf, thinner root casts penetrate enlarged, sediment-filled root casts, and *in situ* breccias commonly accompany these structures. The abundance of root casts increases towards the top of the tidal flat-intervals.

In summary, tidal flat deposits below composite surfaces of the Qishn Formation comprise numerous subenvironments (from shallow subtidal to intertidal to supratidal) with a predominance of supratidal settings, evident from the numerous supratidal features (bird's-eyes, desiccation cracks, tepees, abundant root casts).

Subtidal deposits above composite surfaces

Lagoonal deposits above composite surfaces are bioturbated packstones and grainstones with a diverse open-marine fauna comprising abundant shell debris. Oyster fragments, echinoderms, agglutinating and milioliid foraminifera are the main components of these rocks. Corals, surrounded by a matrix of lagoonal packstones and grainstones, colonize two surfaces. Cross-bedded grainstones and rudstones consisting of peloids, reworked algal lumps and shell debris (mostly rudist debris) overlie four composite surfaces. Bedded oyster floatstones in a matrix of lagoonal packstones were found locally on top of two composite surfaces. All of these sedimentary rocks are shallow subtidal deposits of an open platform with high-energy shoals or protected lagoons (Fig. 3). The investigated composite surfaces thus mark a distinct bathymetric shift from a supratidal to a shallow subtidal environment.

Surface morphology and lateral variability

The morphology of composite surfaces changes within tens of metres from a flat surface to an irregular relief, to an erosive relief, and to a pervasively bored hardground. These surfaces can be impregnated by brownish iron oxides for hundreds of meters. Three types of borings perforate composite surfaces: (i) *Gastrochaenolites*; (ii) tube-shaped borings; and (iii) dense networks of round chambers. *Gastrochaenolites* are clavate, have a single entrance and a size of <1 cm in length and the shape of lithophage bivalves. Lithophage shells, however, are rarely preserved. The moulds are commonly (geopetally) filled with deposits of the same (lagoonal) facies as the overlying beds, or occluded by cement (Fig. 8A). Tube-shaped borings often coexist with lithophage borings. The tubes of 2–3 mm in diameter with a length <1 cm, are often filled with sediment (as described for *Gastrochaenolites*). Remains of the boring organisms were not observed. Considering the shape of the borings, worms are suggested as the producers. Dense networks of small round chambers (1–2 mm in diameter) penetrate discontinuity CS 4. The chambers are connected by thin canals or coalesce to bigger chambers that have geopetal fillings (Fig. 8B). Sharp contacts with the surrounding rock and the shape of the chambers suggest clionid sponges as the producers (Bromley, 1996). Cross-cutting relationships of borings and bored pebbles resulting from reworking of previous hardgrounds are present but rare. Composite surfaces show the highest degree of lateral variability in the study window, as demonstrated along surface CS 5 (Fig. 9).

At Section S001, discontinuity CS 5 has an irregular relief truncating up to 50 cm into the laminated strata below (Fig. 9A). Root casts, abundant tube-shaped and minor *Gastrochaenolites* borings penetrate the surface. Moderately sorted, coarse grainstones mainly consisting of oyster and rudist-shell debris, peloids, and milioliid foraminifera fill the surfical relief, root casts and borings. Grainstone components are the same as those of floatstones, grainstones and rudstones on top of CS 5. The lack of mud and coarse texture of this facies indicates elevated water energy.

At Section S032, 1250 m north of Section S001, the relief and large, sediment-filled root casts found at Section S001 are absent. Instead, there is a 30 cm thick erosive interval that is pervasively bored at the top. Between two and seven generations of shallow, erosive depressions were observed 50 m south and north of S032. Wackestones with little shell debris (including ostracodes) or mudstones with initial glaebules fill these depressions. Glaebules are spherical bodies of 2 mm to 1 cm in diameter consisting of dense, dark brown carbonate micrite with a light brownish outer seam (Fig. 10A). Some glaebules are connected to a coalescing mass, whereas others are clearly isolated by cement-filled, circumgranular cracks. Marine fossils, such as shell fragments are rarely present within the spheres

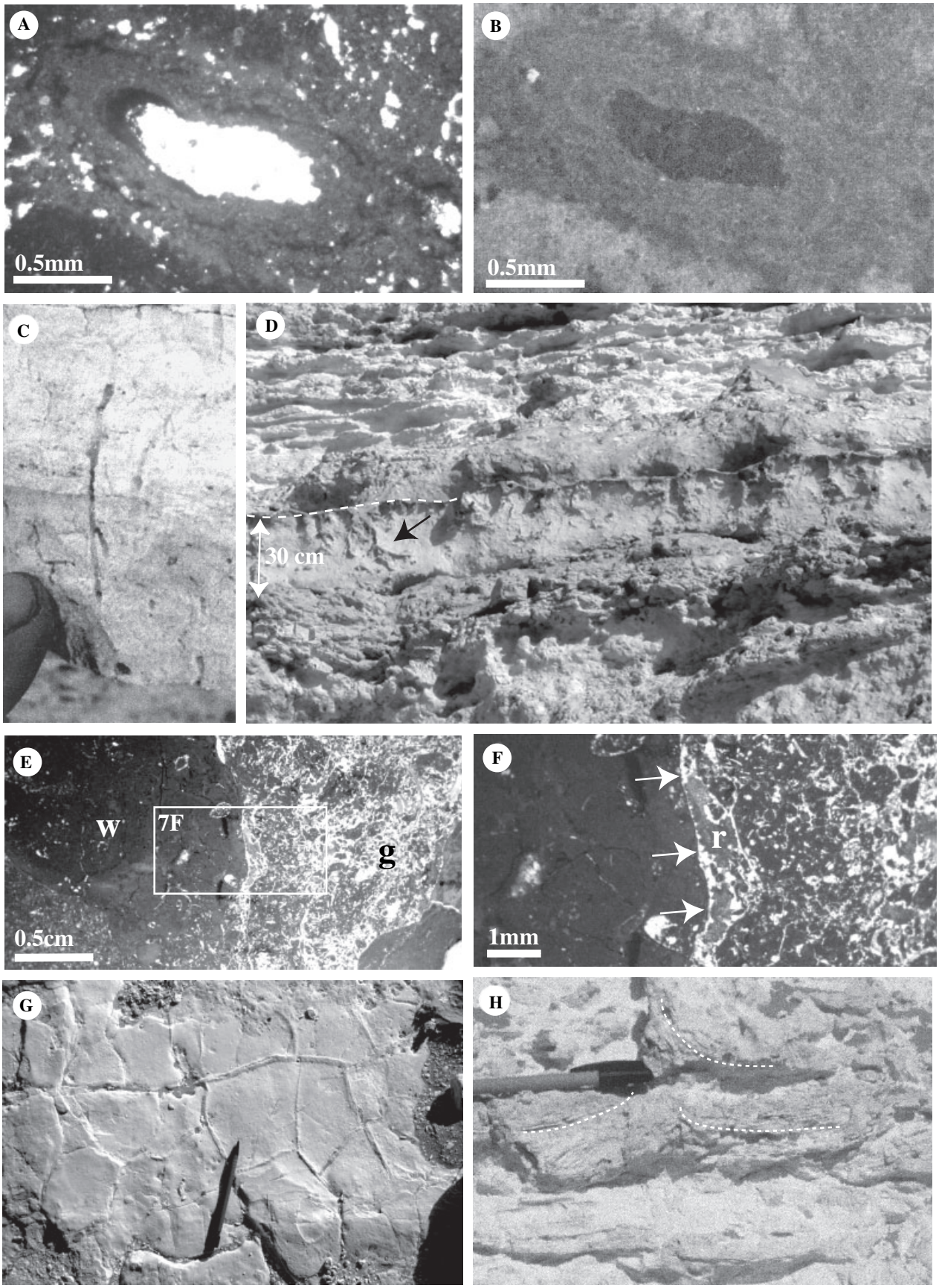
A
0.5mm
B
0.5mm
C
D
30 cm
E
W
7F
g
0.5cm
F
r
1mm
G
H

Fig. 7. Meteoric features. (A) Root cast, occluded by blocky calcite and surrounded by dark sediment with incipient alveolar textures. (B): (A) under cathodoluminescence; (C) downward-bifurcating root cast filled with cement. (D) Composite surface (white, dashed line) penetrated by sediment-filled thick root casts (arrow). (E) Tidal flat wackestone (w) penetrated by root cast filled with grainstone (g). (F) Detail of 7E. Sediment-filled root cast is penetrated by smaller root (r). Small root cast is lined by dog-tooth cement (arrow) and filled with carbonate mud. (G) Polygonal mudcracks on top of tidal flat deposits. (H) Laminated tepee structures on a supratidal mudflat.

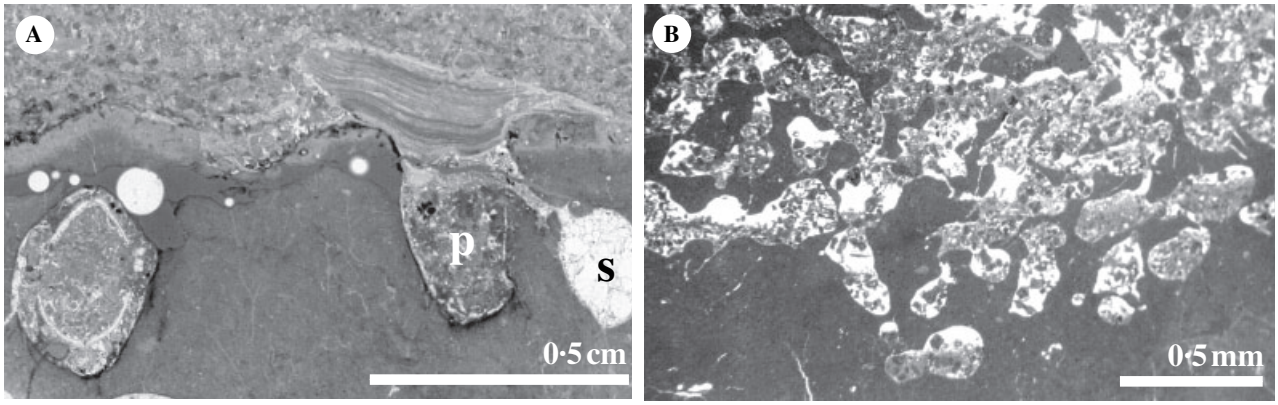

Fig. 8. (A) *Gastrochaenolites borings* penetrating composite surface and muddy sedimentary rock below. Borings are filled with the same bioclastic packstones as occurs overtop (p), or with blocky spar (s). (B) Dense network of geopetally filled clinoiid borings.

(Fig. 10A). Reworking and resedimentation of the underlying strata is indicated by *in situ* or slightly transported breccias that fill the lower portions of the depressions. Desiccation cracks and small root casts perforate surface CS 5 (Fig. 9B).

Eighty metres north of Section S032, CS 5 appears as a flat, sharply cut surface penetrated by tube-shaped and *Gastrochaenolites* borings (Fig. 9C). Locally, these borings have been eroded. In the region around S034, CS 5 appears in the field as a 'regular' bedding plane, meaning a bedding plane which is not bored and is without any features related to subaerial exposure, but has an erosive relief (Fig. 4).

Omission surfaces

Discontinuities with borings, mineralization or increased burrowing below the surface are termed omission surfaces. Encrusting faunas were not observed in the Huqf. Omission-related features are also present, and in some cases even abundant along erosion surfaces and composite surfaces (Fig. 4). In the study window, there is only one extensive omission surface (OS 1), whereas there are 16 laterally limited discontinuities with evidence for omission (Fig. 4).

Laterally limited omission surfaces

Laterally limited omission surfaces are slightly mineralized bedding planes that can be traced for a few meters only, or in some cases for up to 500 m in the outcrop. Omission surfaces are commonly sharp boundaries between different depositional facies types. The intervals below omission surfaces are intensively bioturbated, but the abundance of burrowing decreases laterally within a few tens of meters. Some omission surfaces are locally perforated by tube-shaped and *Gastrochaenolites* borings. The majority of laterally limited omission surfaces were observed in shallow lagoonal settings (blue colours in Fig. 4).

Laterally extensive omission surface

OS 1 is an exceptional omission surface, inasmuch as it is a marker horizon with a lateral extent of 21 km, and it has no lateral variability (Figs 4 and 10C). The surface has an irregular, wavy morphology and marks a bathymetric shift from shallow lagoonal to marly, deeper platform settings. A network of *Thalassinoides* burrows perforates the discontinuity and a 3–4 dm thick interval below. *Thalassinoides* burrows increase in abundance towards the surface. Contacts between burrows and surrounding sediments are sharp, and burrow walls are frequently iron-stained. *Thalassinoides* are filled with fine-grained sedimentary rock, which clearly differs from the surrounding limestone in grainsize and colour, and is weathered out at the present outcrop surface. Burrows, about 5 mm in diameter, also perforate the sediment below OS 1. These burrows do not truncate the discontinuity and are filled with deposits similar to that of the

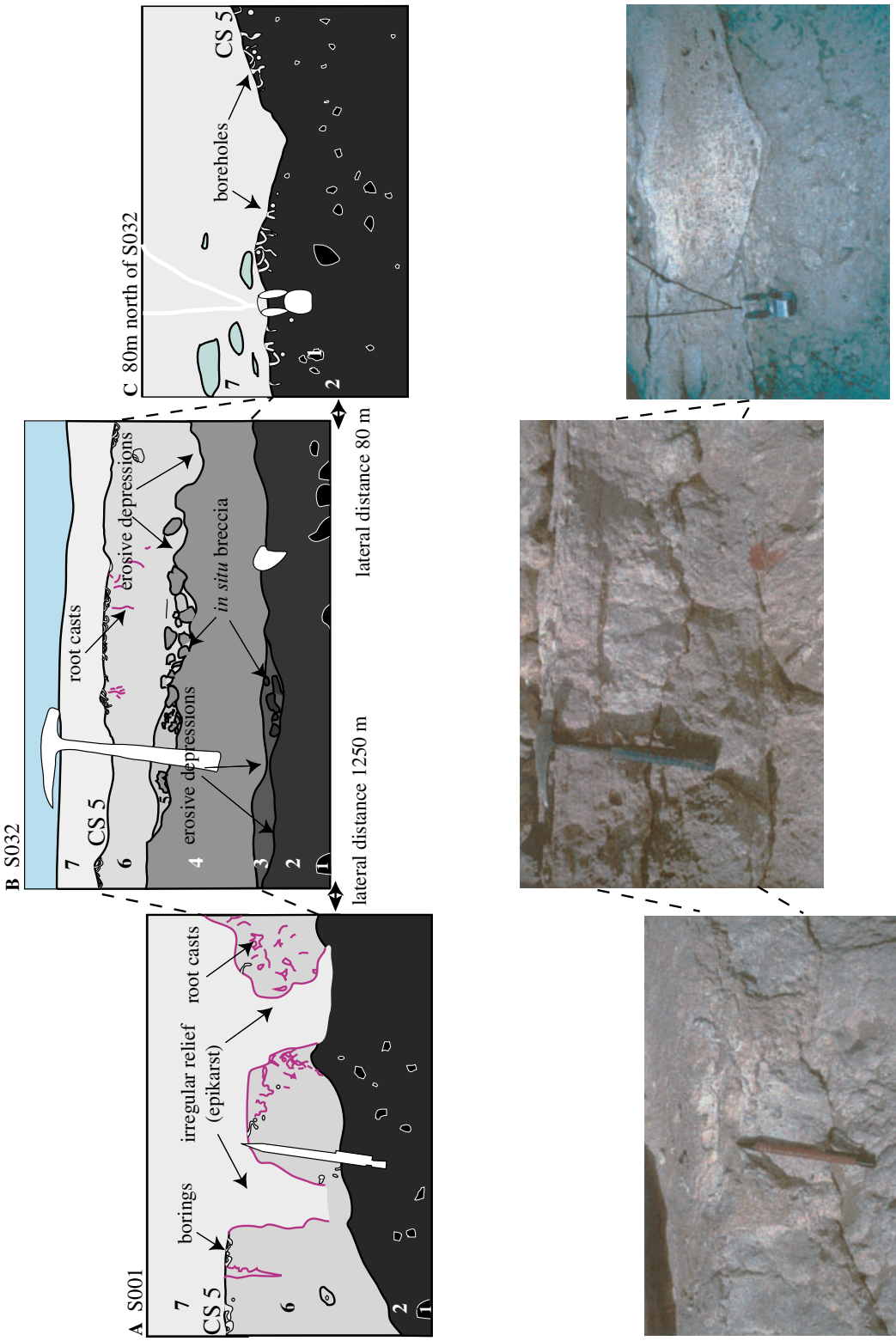

Fig. 9. Lateral variability along composite surface CS 5. Numbers 1 to 7 refer to lithofacies types: 1, *in situ* brecciated limestones; 2, wackestone with thin root casts and desiccation features; 3, wackestone with desiccation features and *in situ* breccia; 4, mudstone with initial glaebules and root casts; 5, *in situ* or slightly transported breccias surrounded by wackestones with desiccation features; 6, wackestone with desiccation features and abundant root casts; 7, medium to coarse grainstone with abundant shell debris and peloids filling epikarstic relief, root moulds and borings. (A) CS 5 has an irregular, epikarstic relief and is penetrated by root casts at Section S001. (B) CS 5 is topping a 30 cm thick erosive interval that is pervasively bored at Section S032. (C) 80 m north of S032, CS 5 is a flat, sharply cut surface penetrated by tube-shaped and *Gastrochaenolites* borings. Locally, these borings have been eroded.

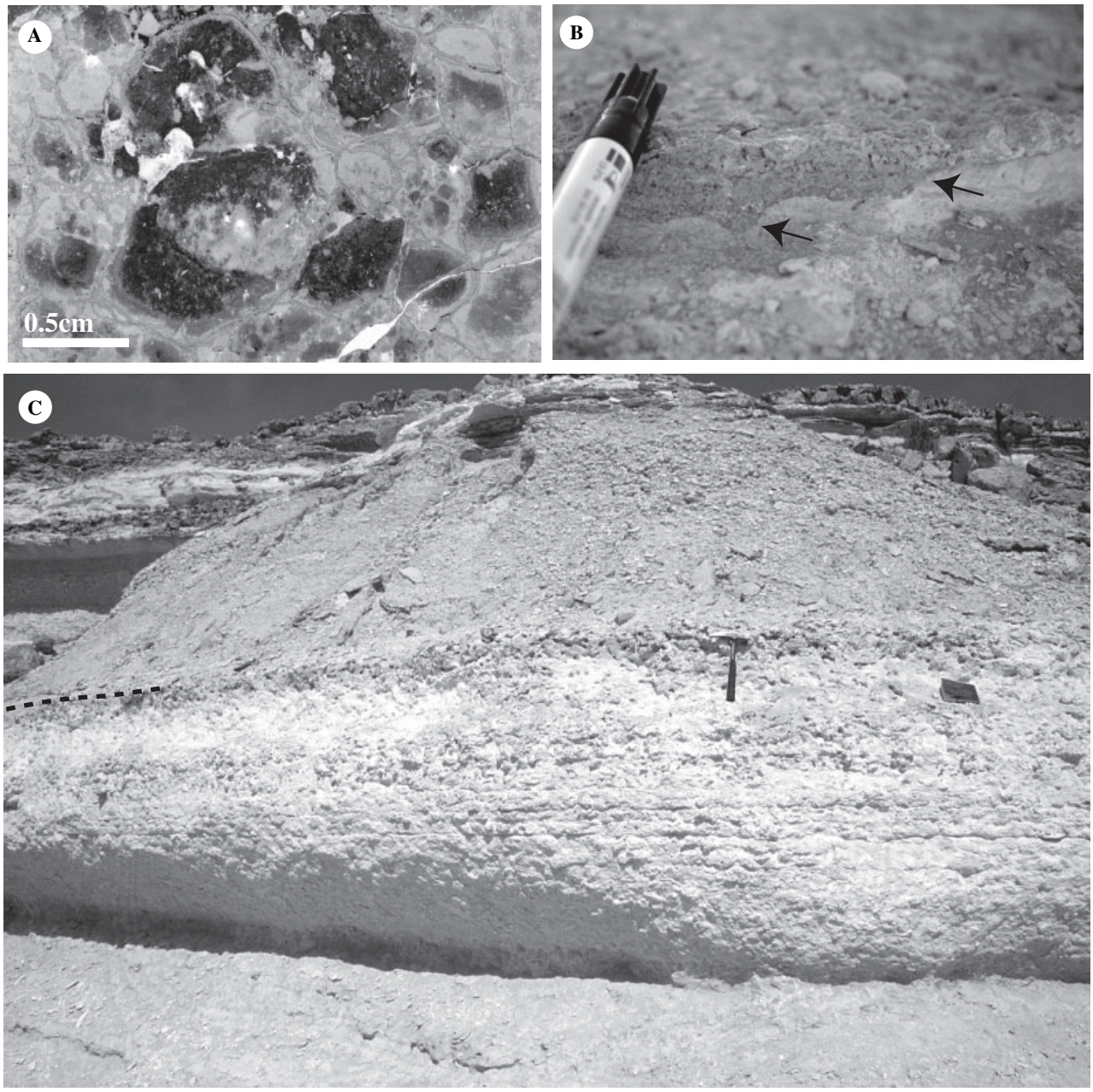

Fig. 10. (A) Incipient glaebules formed by dense, dark micrite with a pale outer seam. (B) Small-scale relief, indicating erosion. (C) Omission surface OS 1 (marked by black-dashed line). Increased bioturbation (open burrows) beneath OS 1 and a sharp facies change across the surface indicate omission.

surrounding sedimentary rock. OS 1 is stained with brownish-red secondary iron oxides (goethite, limonite and siderite) that penetrate 10 cm into the rock. Subrecent gypsum crusts are present along the discontinuity.

Erosion surfaces

A small-scale erosional relief (Fig. 10B), truncated burrows and reworking of underlying strata indicate mechanical erosion along the majority of discontinuity surfaces. These features are also present along composite surfaces (Fig. 4), but here the focus is on erosion surfaces without any petrographic indication for subaerial exposure. Apart from numerous laterally limited erosion surfaces, eight laterally extensive surfaces were observed (ES 1 to ES 8; Fig. 4).

Laterally limited erosion surfaces

Sequence IV consists of cross-bedded shoals of well-washed grainstones, oncoids that resulted

from reworking of *Lithocodium–Bacinella* bindstones, and coarse-grained rudist fragments, indicating wave-controlled, high-energy settings. Sets of cross-bedded deposits truncate each other, resulting in numerous erosion surfaces of very limited lateral extent. These set and coset bounding surfaces are not further considered here.

Apart from Sequence IV, abundant laterally limited erosion surfaces truncate Sequence III, producing a pattern of stacked, laterally discontinuous, thin depositional units. Most of these erosion surfaces are recognized in either intertidal or high-energy settings. In contrast, there are only few laterally limited erosion surfaces in shallow lagoons (indicated with blue colours in Fig. 4) and particularly scarce surfaces in protected low-energy settings. Laterally limited erosion surfaces are absent in relatively deep platform settings deposited below the reach of storm waves (indicated with brown colours in Fig. 4).

Laterally extensive erosion surfaces

Laterally extensive erosion surfaces truncate strata deposited in different lagoonal, tidal flat or high-energy palaeo-environments. Erosion surfaces are frequently located between strata of lower hydrodynamics (below) and elevated energy (above, e.g. ES 7, Fig. 4). Shell lag deposits that fill small erosive depressions are scarcely present. Extensive erosion surfaces are laterally uniform in their morphology and field expression. However, in intervals with stacked thin depositional units (Sequence III), the facies below and above erosion surfaces vary considerably (e.g. ES 3, ES 4, Fig. 4). In contrast ES 1, 2, 6 and 7 have laterally invariable facies below and above the erosion surface (Fig. 4). No angular unconformities are recognized between pre- and post-erosion strata in the Huqf.

GEOCHEMISTRY

Stratigraphic trends in $\delta^{13}C$ and $\delta^{18}O$

Comparison of Huqf geochemical data with northern Oman (Jabal Madar)

Bulk-micrite samples were collected from Section S018 (upper Jurf and Qishn Formations) and from the Kharaib and Shu'aiba Formations at Jabal Madar (Fig. 5) in order to (i) evaluate geochemical evidence for subaerial exposure; and (ii) correlate the sections to the Aptian global chemostratigraphy (Fig. 5; e.g. Menegatti *et al.*, 1998; Weissert *et al.*, 1998; Bralower *et al.*, 1999; Jenkyns & Wilson, 1999).

With reference to oxygen-isotope values, mean bulk-micrite data from S018 and from Jabal Madar are as low as −4·8‰ [$n = 138$, standard deviation (s) = 1·5‰] and −6·6‰ ($n = 99$, $s = 1{\cdot}7$‰), respectively. Overall, an upward trend to lower values is observed in Section S018 superimposed by a number of smaller shifts to low values. The same pattern is visible at Jabal Madar (northern Oman) but here, amplitudes of superimposed shifts are considerably higher (Fig. 5).

With respect to carbon-isotope data, two intervals with low $\delta^{13}C$ values (corresponding to Sequence I and portions of Sequence III in Fig. 5) are present in Section S018 ($\delta^{13}C = -1{\cdot}6$‰, and −1·1‰, respectively). Between Sequence I and Sequence III there is a stratigraphic interval of 8 m with higher carbon-isotope values (largely Sequence II in Fig. 5; mean of 1·1‰). Mean $\delta^{13}C$ from Section S018 are −0·8‰ ($n = 138$, $s = 1{\cdot}5$‰), i.e. considerably low compared with Jabal Madar data ($\delta^{13}C = 1{\cdot}7$‰, $n = 99$, $s = 1{\cdot}4$‰). An exception is Sequence II, characterized by mean values oscillating around 1·5‰ (s = 1·3‰, Fig. 5).

The upper portions of Sequence IV in Section S018 (above ES 5, Fig. 5) are characterized by irregular, ^{13}C-depleted values around −3·8‰. This interval corresponds to tightly cemented, fully lithified intervals forming the top of table mountain exposures that have undergone pervasive Holocene karstification (Immenhauser *et al.*, 2004). Therefore, this portion of the section and the corresponding isotope data are not further considered here.

Comparison of isotope data from different carbonate phases

In Fig. 11A, micrite $\delta^{13}C$ and $\delta^{18}O$ from Section S018 are compared with values from different calcite cements and two bivalve shells (an oyster and a rudist). Cement phases include fracture fillings and non-luminescent, blocky calcites filling intergranular pores, borings, and meteoric features. These later cements are here referred to as 'meteoric cements'. Meteoric features include bird's-eyes, root casts, sheet cracks, and circumgranular cracks. Meteoric cement $\delta^{13}C$ and $\delta^{18}O$ have a wide range compared with other cement phases and micrites, but they generally display the lowest values (Fig. 11A). Burrows, borings and meteoric features are often infilled by sediments plotting in the same $\delta^{13}C$ and $\delta^{18}O$ field as bulk micrites from S018 (Fig. 11B).

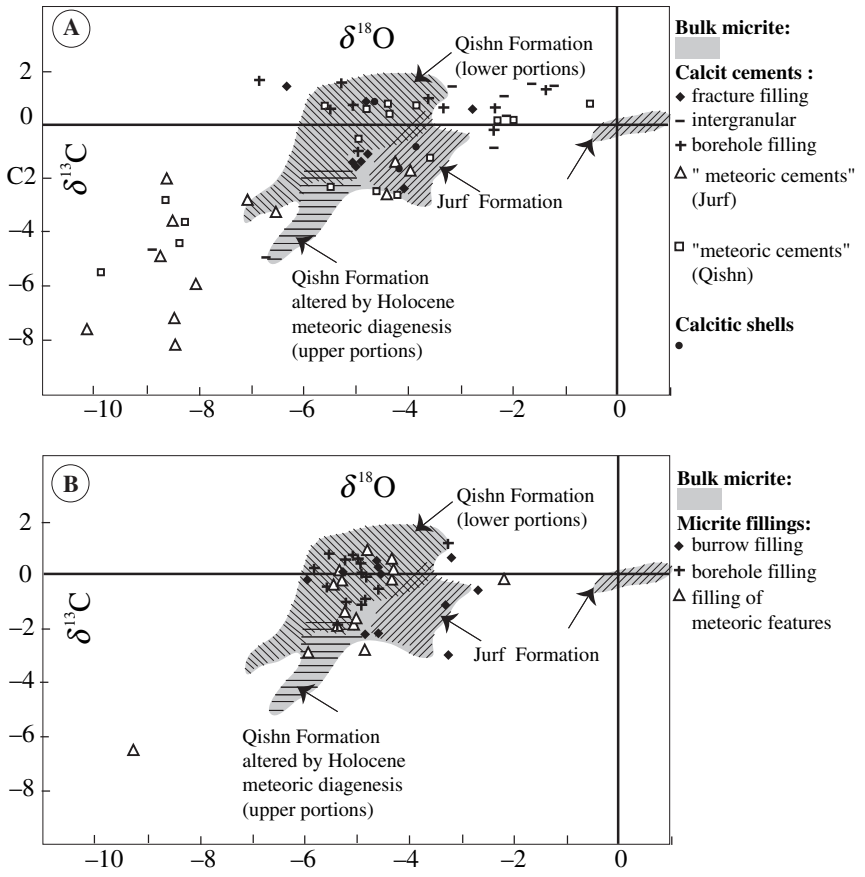

Fig. 11. (A) Comparison of bulk micrite δ^{13}C and δ^{18}O from Section S018 (grey field) with values from different calcite cements and bivalve shells (oysters, rudists, black symbols). Meteoric cement δ^{13}C and δ^{18}O have a wide range compared with other cement phases and micrites, but they generally display the lowest values. (B) Comparison of bulk micrite δ^{13}C and δ^{18}O sampled from within burrows, borings and meteoric features (black symbols) and bulk micrite from Section S018 (grey field). Both plot in the same field.

Interpretation and discussion

In Section S018, two intervals with low δ^{13}C are present (Sequences I and III, Fig. 5). A similar pattern but with different absolute values was observed at Jabal Madar (interval corresponding with Sequence III, Fig. 5). Several mechanisms can explain these low values but the quantification of the effects of each individual factor is difficult.

First, Cretaceous sea water 'ageing' related to long residence time of water masses in shallow, poorly circulated settings such as documented for the Qishn Formation (Immenhauser *et al.*, 2004) can result in low δ^{13}C. The process of sea water ageing refers to the progressive uptake of increasing amounts of ^{13}C-depleted carbonate as the result of oxidation of organic matter (see *Discussion* in Patterson & Walter, 1994; Immenhauser *et al.*, 2003).

Second, numerous meteoric features (epikarst, root casts, glaebules, alveolar structures) in Sequences I and III point to repeated subaerial exposure events within these intervals. Depletion in ^{13}C resulting from the input of isotopically light soil-zone CO_2 (e.g. Allan & Matthews, 1982; Tucker & Wright, 1990; Joachimski, 1994; Immenhauser *et al.*, 2002) might have further lowered bulk micrite values in these intervals.

Third, δ^{13}C-fluctuations in Aptian global seawater geochemistry (Menegatti *et al.*, 1998 and references therein) might be recorded in the carbon-curves in the Huqf and at Jabal Madar. Based on the Cismon core data, Menegatti *et al.* (1998) divided the Aptian δ^{13}C stratigraphy of the Alpine Tethys into eight chemostratigraphic segments (C1–C8). The Selli event (OAE1a) is contained in segments C4 through C6. The same chemostratigraphic pattern was recognized from the Aptian Shu'aiba Formation of the subsurface of Oman (Vahrenkamp, 1996; see *Discussion* in Immenhauser *et al.*, 2005). Based on strontium-isotope and biostratigraphic data from the Qishn Formation, Immenhauser *et al.* (2004, 2005) concluded that the segment C7, i.e. shift towards higher δ^{13}C values above the Selli event, is stratigraphically not reached in the Huqf. Strontium-isotope and biostratigraphic data imply that the pronounced shift to lower carbon values in Sequence III of the Qishn Formation (Fig. 5) correlates with the C3 segment of Menegatti *et al.* (1998). The preservation of the C3 segment in the Qishn Formation is, however, ambiguous because

the sedimentary rock was deposited on a restricted carbonate platform and altered by meteoric diagenesis. The chemostratigraphic section on Jabal Madar, however, is interpreted as stratigraphically reaching segment C7 (Fig. 5).

Subsequent lithification in the burial environment mainly affects the oxygen isotopic record (e.g. Banner & Hanson, 1990; Veizer *et al.*, 1999), and is not considered as a main controlling factor for carbon isotope geochemistry. Regional evidence clearly indicates that the burial depth of the Qishn limestones was as shallow as 200 m (±50 m, Immenhauser *et al.*, 2004), as opposed to the roughly 10 km of burial depth of coeval stratigraphic units in the northern Oman Mountains (e.g. Glennie *et al.*, 1974; Immenhauser *et al.*, 2000). Jabal Madar, located at the edge of the northern Oman allochthonous units has seen intermediate burial depths. The shallow burial of the Qishn Formation is here supported by the conspicuous absence of burial cements in 395 thin sections that have been analysed with standard and cathodoluminescence microscopy and by the absence of stylolites. Clearly, this implies that burial fluids were not a main controlling factor of the Qishn Formation carbonate geochemistry. The effects of Cretaceous meteoric diagenesis, however, have to be considered when discussing $\delta^{18}O$ trends.

The oxygen-isotope values of Huqf micrites are low compared with Middle Cretaceous open oceanic sea water data from foraminifera or aragonitic marine cements (e.g. Norris *et al.*, 2001; Pearson *et al.*, 2001), but more comparable to relatively 'light' coastal marine seawater values from pristine low-Mg calcite rudist shells ($\delta^{18}O$ between −1 and −5‰, Steuber, 2002). Obviously, in the absence of significant burial diagenesis, micrite $\delta^{18}O$ values as low as −8‰ (Fig. 5) and meteoric cements as low as −10‰ (Fig. 11A) are related to ^{18}O-depleted rainwater (e.g. Allan & Matthews, 1982). These values are comparable with isotopic data from Albian meteoric cements in northern Oman (−6 to −8‰; Immenhauser *et al.*, 2000). For comparison, present day rainwater $\delta^{18}O$ in Oman is as low as −5 to −7‰ [standard mean ocean water (SMOW)], which roughly translates into meteoric calcite values of −5·3 to −7·3‰ (VPDB, Clark & Fontes, 1990). Both the S018 and the Jabal Madar section (Fig. 5) display a variant $\delta^{18}O$ pattern with saw-tooth-shaped excursions. This is not in agreement with a pervasive meteoric overprint leading to invariant $\delta^{18}O$ and variant $\delta^{13}C$ (the 'meteoric water lines' of Lohman, 1988). In contrast, the observed chemostratigraphic pattern suggests the superposition of episodes of meteoric diagenesis related to specific subaerial exposure horizons.

Although a number of factors and processes are superimposed in the geochemical signal of the Qishn, the authors conclude that subaerial exposure as evidenced from numerous sedimentologic features is further supported by shifts to low $\delta^{13}C$ and from generally low (but variable) $\delta^{18}O$ values of bulk micrite. Moreover, meteoric cements, which are strongly depleted in ^{18}O and ^{13}C point to subaerial conditions.

DISCUSSION AND INTERPRETATION

Definition of long-term/terrestrial and intermittent subaerial exposure

The terms 'terrestrial' and 'intermittent' subaerial exposure are differentiated here based on the exposure index (a percentage of time an area is exposed to subaerial conditions) of Ginsburg *et al.* (1977) established on the recent tidal flats of Andros Island. The terrestrial exposure environment has an exposure index of 100%, and normally is not flooded by marine waters (exceptions are major hurricane floods). Different types of soils, terrestrial plants and karst can develop in the terrestrial environment, depending on climate, hydrology, lithology and topography. The supratidal environment and intertidal environments are exposed to intermittent subaerial conditions that are too short for the development of terrestrial plants, soils and karst.

Generation of composite surfaces

Desiccation cracks, bird's-eyes and root casts can be related to the tidal environment, and do not necessarily require terrestrial conditions (Fig. 12A). However, alveolar textures and incipient glaebules as observed below CS 5 indicate soil development and thus terrestrial subaerial exposure (Esteban & Klappa, 1983). The formation of scarce glaebules in the Qishn Formation can express only incipient soil development. Another possibility is that a soil with different soil-horizons was eroded and only incipient glaebules from the transition horizon were preserved. Here, the latter possibility is favoured, because all glaebules were found in topographic depressions, sheltered from erosion.

Early diagenetic cements in meteoric features that are significantly depleted in ^{13}C and ^{18}O also

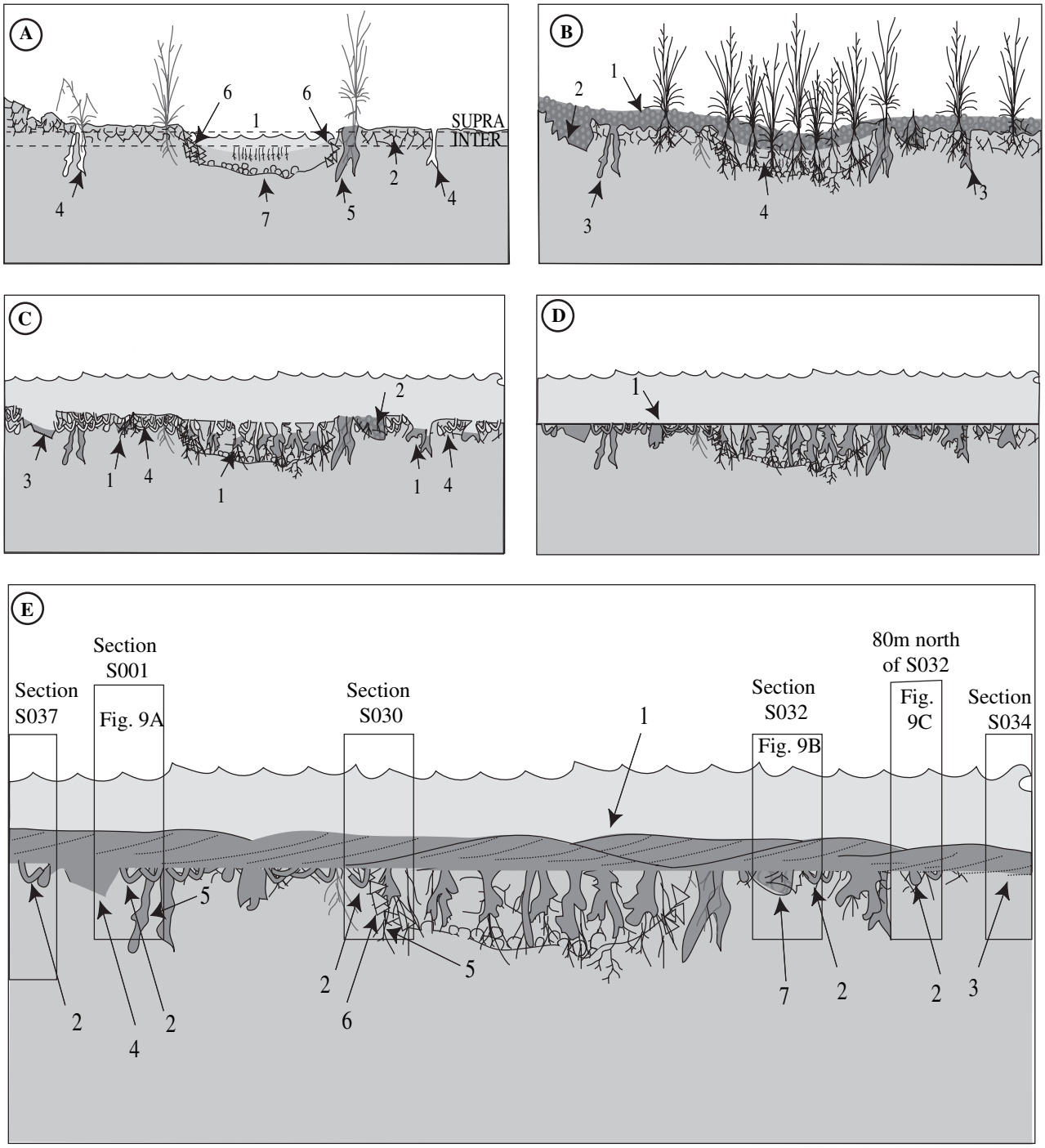

Fig. 12. Schematic model for the generation of a composite surface; (A) Tidal flat environment, with closely spaced subenvironments: 1, swamp plants; 2, desiccation cracks; 4, enlarged root casts; 5, root casts filled with high-energy sediments, and penetrated by another generation of roots; 6, locally restricted erosion; 7, *in situ* breccia. (B) Terrestrial subaerial exposure: 1, soil cover; 2, epikarst; 3, enlarged, sediment-filled root casts; 4, plants (abundant on former tidal channels). (C) Marine flooding removed soil and vegetation: 1, enlarged root casts; 2, soil-remnants (preserved in depressions sheltered from erosion). 3, epikarstic relief (partly eroded and partly filled with high-energy deposits); 4, boring organisms (pervasively penetrating early lithified rock). (D) Wave induced abrasion of fully lithified, pervasively bored rock, results in flat surface (1). (E) Composite surface CS 5 as observed in different sections: 1, subtidal shoals of high-energy grainstones; 2, borings; 3, flat surface where meteoric features and borings have been eroded; 4, epikarst; 5, root casts; 6, local breccias; 7, soil-remnants (glaebules) in sheltered depression.

point to terrestrial conditions. The same holds true (with some restrictions) for intervals with abundant meteoric features combined with low carbon values (Sequences I, III; Fig. 5) and generally low oxygen values in the Huqf. Different processes can result in an irregular relief as observed along composite surfaces: (i) patchy lithification and subsequent, submarine erosion (Hillgärtner, 1998); (ii) bioerosion, wave action and seawater spray in the inter- and supratidal environment including rocky coastlines (coastal karst or syngenetic karst *sensu* Sweeting, 1979); and (iii) carbonate solution under meteoric conditions (terrestrial epikarst *sensu* Esteban & Klappa, 1983). Coastal and submarine erosion (i, ii) resulting in the above-described irregular relief cannot be ruled out. Because of the abundance of root casts and some glaebules in close vicinity to the irregular relief, a meteoric origin (terrestrial epikarst) is proposed here. The abundance of root casts increases towards the top of the tidal flat environment, suggesting that these intervals were exposed to subaerial conditions for a longer time period relative to stratigraphically lower portions. In summary, there is sufficient petrographic and geochemical evidence for terrestrial subaerial exposure of composite surfaces and underlying tidal flats (Fig. 12B).

Flooding of the subaerially exposed environment (Fig. 12C) is evident from the subtidal deposits found on top of composite surfaces. Transgressive deposits, vegetation and soil-horizons have probably been removed during flooding, but root casts and some glaebules are preserved. Consequently composite surfaces separate supratidal and subtidal facies without any transition between the two. Comparable, rapid vertical successions characterize 'transgressive ravinement surfaces' (e.g. Swift, 1968, 1978; Swift *et al.*, 2003). Information on depositional geometries is, however, insufficient to classify composite surfaces of the Qishn Formation as transgressive ravinement surfaces.

In the Huqf, different organisms including clinoiid sponges pervasively penetrate the sea floor, indicating that it was consolidated during early diagenesis. Moreover, modern analogues suggest that borings produced by clinoiid sponges are indicative of fully lithified rocks (Bromley, 1996). Early-diagenetic lithification can be related to the supratidal and terrestrial environment or to the subtidal as described by Shinn (1969) from the present-day Arabian Gulf (formerly 'Persian Gulf'). Cementation of the carbonate seafloor in the Arabian Gulf is mainly controlled by the sedimentation rate and the grain size that influences the porosity/permeability properties of the sediment (Shinn, 1969). Using the modern Arabian Gulf as an analogue (Shinn, 1969), the tidal flat sediments (mudstone, wackestones, fine-grained packstones and grainstones) of the Huqf appear too fine-grained for early submarine cementation. Consequently, early cementation in the Huqf is preferably related to the supratidal environment or terrestrial exposure. Petrographic studies of the tidal rocks showed that the majority of the cements are non-luminescent, blocky calcites, which can form in different diagenetic environments, but are typical of meteoric settings (Tucker & Wright, 1990).

Locally, composite surfaces of the Huqf have a sharply cut, flat morphology. High-energy abrasion of fully lithified, pervasively bored sedimentary rocks in a shallow-marine environment, typically forms flat surfaces (Hillgärtner, 1998) as observed in the Huqf (Fig. 12D). Differential erosion postdating boring activity locally erased borings along composite surfaces and completely removed them along discontinuities SE 1 and SE 2. Erosion on a larger scale is evident from the entirely eroded tidal flat intervals. This is documented below CS 3 between Section S037 and S031 (Fig. 4), where tidal flat deposits, including root casts and borings on top are missing.

Lateral variability – causes and impact

Although modern tidal flat environments have little topographic relief, they bear an internal topography with many subenvironments, such as tidal channels, beach ridges, levees, ponds and islands (e.g. Shinn *et al.*, 1965; Shinn, 1969; Gebelein, 1974; Ginsburg *et al.*, 1977; Shinn, 1983; Wilkinson *et al.*, 1996, 1997; Rankey, 2002). These subenvironments are exposed to subaerial conditions with variable duration (exposure index of Ginsburg *et al.*, 1977). Consequently, the intensity of desiccation and sediment reworking varies across modern tidal flat environments (Hardie & Shinn, 1986), which makes them prone to differential erosion. Similar to the modern analogues, the depositional environment in the Huqf included supratidal flats, intertidal settings and tidal channels (Fig. 12A). Desiccation structures (e.g. circumgranular cracks, polygonal mudcracks, Figs 4 and 7G) vary in abundance below and at the composite surfaces of the Qishn Formation, suggesting an environment that is prone to differential erosion. For example, differential erosion was observed along

CS 5 around Section S032, where between two and seven erosive depressions cross-cut each other (Fig. 9B). Eighty metres further to the north, this interval is eroded (Fig. 9C). Lateral variability along the surface is thus related to the depositional environment below.

In modern carbonate environments, supratidal flats can become consolidated and cemented within only a few years (Shinn, 1983). Similar cementation rates applicable for the Qishn Formation might explain why root casts are more abundant on top of tidal channels compared to supratidal flats (Fig. 12A and B). Channel-fillings might still have been soft during plant-colonization, whereas mudflats and sandflats were already consolidated or even lithified in the supratidal and later terrestrial environment. Although root casts are partly related to terrestrial conditions the tidal flat environment influences their variable distribution and thus causes lateral variability along/below composite surfaces.

Lateral variability along composite surfaces is, however, not only due to the facies below, but is also influenced by terrestrial subaerial exposure creating an epikarstic relief, and to erosion which is related to the flooding of the subaerially emerged platform (Fig. 12B and C). Transgression partly removed the epikarstic relief, borings and root casts. This resulted in a discontinuity appearing as a subaerial exposure surface with an epikarstic relief in one place, as a pervasively bored hardground in another and as a flat abrasion surface in yet a third place (Fig. 9). Spatially separated two-dimensional sections or cores would only show one part of the succession of processes that altered the carbonate platform (Fig. 12E). This can result in misinterpretations, especially in the interior of extensive flat platform tops, where stratal geometries are subtle. For example, in Section S037 and Section S032 (Fig. 12E) a bored discontinuity is preserved that is easily misinterpreted as a submarine hardground, lithified and bored because of sediment starvation during maximum flooding. Sections S001, S030 and S032 (Fig. 12E), on the other hand show that the carbonate platform was exposed to terrestrial conditions and the discontinuity would thus represents a sequence boundary.

Allocyclic versus autocyclic origin

Composite surfaces were exposed to terrestrial conditions, including the development of a soil and an epikarstic relief. Terrestrial subaerial exposure of carbonate platforms is indicative for relative sea level lowering, and cannot be produced by autocyclic processes or changes in sediment supply (Schlager, 1993). Consequently, meteoric alteration of a carbonate platform is a marker for allogenic forcing of the sedimentary system (Strasser, 1991). Therefore, it is crucial for the reconstruction of ancient sea-level fluctuations and sequence stratigraphic interpretations to differentiate between structures that point to intermittent and terrestrial subaerial exposure.

Sedimentary structures and composition of rocks above composite surfaces point to a mean palaeo-water depth of >10 m (Figs 3 and 4). Thus, palaeo-water depth increases from terrestrial exposure to more then 10 m across composite surfaces. Composite surfaces and the accompanying bathymetric shifts were regionally correlated for up to 170 km (to Jabal Madar, Fig. 5). This suggests that the depositional profile across the discontinuities (and its lateral extent) documents a regional transgression, as opposed to lateral shifts of sediment bodies. Consequently, composite surfaces are of allocyclic origin and record a regional regression followed by a transgression.

Omission surfaces

Increased bioturbation and borings (although scarce) suggest sediment starvation along laterally limited omission surfaces. Clari *et al.* (1995) pointed out that the non-Waltherian superposition of different strata suggests an interruption in sedimentation such as omission or erosion. The superposition of different depositional facies across distinct surfaces in the Huqf thus gives additional indication for omission. Laterally limited omission surfaces are restricted to open lagoonal settings, which suggest that these discontinuities record local processes such as sediment starvation due to local currents in this particular environment. In depositional environments with a higher hydrodynamic level, omission surfaces are absent. This is perhaps due to high sedimentation and erosion rates in more open lagoonal settings.

Facies shifts across OS 1 that extend for at least 21 km mark a shift in palaeo-water depth from shallow lagoonal to marly, open platform conditions, with higher water depth (Fig. 4). The sequence-stratigraphic interpretation of the Qishn Formation shows that the deepening trend across this discontinuity records the maximum flooding of a regional transgression (allocyclic, Immenhauser *et al.*, 2004). Increased

density of *Thalassinoides* burrows below OS 1 causes the irregular wavy morphology of the surface and points to low sedimentation rates. Sharp contacts between burrow fillings and surrounding sediment is evidence that the sediment around burrows was at least 'firm' when infilled (Bromley, 1975). Iron-staining of *Thalassinoides* walls might be caused by both Barremian omission prior to burrow-filling and/or exposure to present-day desert climate. Brownish impregnation of the discontinuity surface might result from subrecent to recent fluid flow along a flow barrier (the marly sediment above), which is highlighted by gypsum crusts along the surface. Mineralization of the surface during Barremian/Aptian omission, however, can result in a comparable impregnation (Gomez & Fernandez-Lopez, 1994). The lack of lateral variability along OS 1 is explained by the protected lagoonal setting with a low hydrodynamic level. Moreover, the marly deeper-marine platform sediments deposited above OS 1 suggest only minor subsequent erosion.

Erosion surfaces

The abundance of laterally limited erosion surfaces is closely related to the depositional environment. In Sequence III, numerous subtidal and tidal shoals truncate strata below, resulting in laterally limited erosion surfaces. The abundance of laterally limited erosion surfaces decreases with the hydrodynamic intensity. Only few erosion surfaces are recognized in shallow open lagoons. They are rare in protected low-energy environments and missing in deeper platform settings below the reach of storm waves.

Besides the large number of laterally limited erosion surfaces, eight laterally extensive surfaces were observed, which are not bound to specific depositional environments. Consequently, local currents are not likely to have generated these discontinuities. In contrast, regional transgressions might have produced laterally extensive erosion surfaces (allocyclic). This is in accordance with sequence stratigraphic interpretations of laterally extensive erosion surfaces correlatable across a N–S transect of 100 km in the Huqf area (Immenhauser *et al.*, 2004).

A sharp facies change occurs across six erosion surfaces suggesting that a transitional interval between sedimentary rocks of different depositional environments possibly was eroded, or sediments were never deposited. Decreasing $\delta^{13}C$ and $\delta^{18}O$ values below some erosion surfaces (ES 1 in the Huqf and DsG at Jabal Madar; Fig. 5) imply that the missing intervals might have been exposed to subaerial conditions. Shell lag deposits in small erosive depressions could be indicative of storm scouring but the evidence is subtle. The lack of angular unconformities between strata below and above extensive erosion surfaces can be explained by the orientation of the study-window parallel to regional facies belts of the palaeo-environment.

The lateral variability of an erosion surface in terms of facies below and above the discontinuity varies considerably in intervals where stratigraphically thin successions of differing facies overlie each other (Sequence III; Fig. 4). In such settings, only minor (differential) erosion can remove one or several of these successions from some sections, whereas the same intervals might be preserved in others.

In the Huqf, palaeo-depositional environments with a topographic relief (open platform with shoals, coral and rudist biostromes; Fig. 3) show higher facies variability compared with deeper settings with low relief. Consequently, facies below erosion surfaces capping a topographic relief change laterally (e.g. ES 4; Fig. 4), whereas those in low-energy, low-relief, deeper settings with a flat topography and low water energy are laterally uniform (e.g. ES 1, ES 5; Fig. 4). The topography, the hydrodynamic level and the available accommodation space of the depositional environment prior to erosion thus might influence differences in the facies contrast across erosion surfaces.

SUMMARY AND CONCLUSIONS

In the Barremian to Lower Aptian Qishn Formation of Oman, 17 laterally extensive discontinuities record relative, regional sea-level fluctuations and are thus of allocyclic origin. In contrast, 43 laterally limited discontinuities record locally active processes such as from storm currents or waves. The exceptionally well-exposed Qishn Formation allows for a lateral study of these surfaces. The results of this study offer a more detailed insight into the recognition and origin of discontinuity surfaces in shallow marine carbonate settings. This can be extrapolated to subsurface core studies or studies based on spatially separated one-dimensional outcrop sections in comparable depositional environments. Three surface types were differentiated and interpreted within the Qishn Formation:

- Six laterally extensive composite surfaces record regional exposure and terrestrial modification of a tidal flat environment and subsequent flooding. Petrographic evidence for terrestrial conditions is supported by negative shifts in $\delta^{13}C$ values of bulk micrite and calcite cements and overall low $\delta^{18}O$ values. The high degree of lateral variability along and below composite surfaces is due to rapid and small-scale lateral facies changes in the underlying tidal flat environment, meteoric alteration during terrestrial subaerial exposure and to differential erosion during subsequent flooding.
- Laterally limited omission surfaces restricted to open lagoonal settings are probably the result of sediment starvation due to local processes, such as wave or storm currents. One laterally extensive omission surface records maximum regional transgression. This discontinuity exhibits no lateral variability reflecting the underlying environment and the lack of differential erosion postdating omission.
- Numerous, laterally limited erosion surfaces are related to local processes in distinct depositional environments and they decrease with hydrodynamic energy. Eight laterally extensive erosion surfaces mark the onset of regional transgressive pulses. The lateral variability of erosion surfaces in terms of facies below and above is high in intervals with stacked, thin depositional units. Moreover, lateral variability is related to the topography and the hydrodynamic level of the depositional environment prior to erosion.

ACKNOWLEDGEMENTS

The authors thank Petroleum Development Oman for financial support of this study and the Ministry of Oil and Gas of the Sultanate of Oman for permission to perform fieldwork in the Haushi-Huqf area. Fieldwork at Jabal Madar was financially supported by Shell-Rijswijk. U. S. acknowledges partial funding by *ISES* (Netherlands Research Centre for Integrated Solid Earth Science). We are indebted to B. v/d Kooij, E. van Bentum, K. Verwer, G. de Bruin and B. Heesbeen for their contribution during fieldwork. W. Schlager is acknowledged for his comments on earlier versions of this manuscript and fruitful discussions on modern tidal flat environments. We thank A. Wright for revision of the English text. H. Vonhof and R. Kaandorp are acknowledged for their help in the stable-isotope laboratory and W. Lustenhouwer for his support in the optical laboratory. We thank N. Koot and B. Lacet for their assistance in preparing thin sections. We also would like to thank reviewers P. Homewood and J. Amthor and editor I. Montañez for their highly appreciated, helpful comments. This is publication 2004·04·03 of Netherlands Research School of Sedimentary Geology (NSG).

REFERENCES

Allan, J.R. and **Matthews, R.K.** (1982) Isotope signatures associated with early meteoric diagenesis. *Sedimentology*, **29,** 797–817.

Alsharan, A.S. and **Nairn, A.E.M.** (1997) *Sedimentary Basins and Petroleum Geology of the Middle East*. Elsevier, Amsterdam, 843 pp.

Banner, J.L. and **Hanson, G.H.** (1990) Calculation of simultaneous isotopic and trace element variations during water-rock interaction with applications to carbonate diagenesis. *Geochim. Cosmochim. Acta*, **54,** 3123–3137.

Beydoun, Z.R. (1964) The stratigraphy and structure of the Eastern Aden Protectorate, Overseas Geology and Mineral Resources, London. *Bulletin Supplement*, **5,** 107.

Bralower, T.J., CoBabe, E., Clement, B., Sliter, W.V., Osburn, C.L. and **Longoria, J.** (1999) The record of global change in Mid-Cretaceous (Barremian-Aptian) sections from Sierra Madre, northeastern Mexico. *J. Foraminifera Res.*, **29,** 418–437.

Bromley, R.G. (1975) Trace fossils at omission surfaces. In: *The Study of Trace Fossils* (Ed. R.W. Frey), pp. 399–428. Springer-Verlag, New York.

Bromley, R.G. (1996) Trace fossils. In: *Encyclopedia of Earth Sciences* (Ed. E.J. Dasch), pp. 1105–1108. Macmillan, New York.

Cander, H. (1995) Interplay of water-rock interaction efficiency, unconformities, and fluid flow in a carbonate aquifer: Florida aquifer: Floridan aquifer system. In: *Unconformities and Porosity in Carbonate Strata* (Eds D.A. Budd, A.H. Saller and P.M. Harris), *AAPG Mem.*, **64,** 103–124.

Clari, P.A, Dela Pierre, F. and **Martire, L.** (1995) Discontinuities in carbonate successions: identification, interpretation and classification of some Italian examples. *Sed. Geol.*, **100,** 97–121.

Clark, I.D. and **Fontes, J.C.** (1990) Paleoclimatic reconstruction in northern Oman based on carbonates from hyperalkaline groundwaters. *Quatern. Res.*, **33,** 320–336.

Dunham, R.J. (1969) Early vadose silt in Townsend mound (reef), New Mexico. In: *Depositional Environments in Carbonate Rocks* (Ed. G.M. Friedman), *Spec. Publ. Soc. Econ. Paleont. Miner.*, **14,** 139–182.

Esteban, M. (1974) Caliche textures and Microcodium. *Boll. Soc. Geol. Ital.*, **92** (Suppl.), 105–125.

Esteban, M. and **Klappa, C.F.** (1983) Subaerial exposure environment. In: *Carbonate Depositional Environments* (Eds P.A. Scholle, D.G. Bebout and C.H. Moore), *AAPG Mem.*, **33,** 1–54.

Fouke, B.W., Everts, A.W., Zwart, E.W., Schlager, W., Smalley, P.C. and **Weissert, H.** (1995) Subaerial exposure unconformities on the Vercors carbonate platform (SE France) and their sequence stratigraphic significance. In: *High*

Resolution Sequence Stratigraphy: Innovations and Applications (Eds J.A. Howell and J.F. Aitken), *Geol. Soc. Spec. Publ.*, **104,** 295–320.

Freytet, P. and **Plaziat, J.C.** (1982) Continental Carbonate Sedimentation and Pedogenesis – Late Cretaceous and Early Tertiary of Southern France. *Contrib. Sedimentol.*, **12,** 213.

Gebelein, C.D. (1974) *Guidebook for Modern Bahamian Platform Environments*. Geol. Soc. Am. Annual Meeting. Fieldtrip Guide, St. George, 93 pp.

Geel, T. (2000) Recognition of stratigraphic sequences in carbonate platform and slope deposits: empirical models based on microfacies analyses of Paleogene deposits in southeastern Spain. *Paleogeogr. Paleoclimatol. Paleoecol.*, **155,** 211–238.

Ginsburg, R.N., Hardie, L.A., Bricker, O.P., Garrett, P. and **Wanless, H.R.** (1977) Exposure index: a quantitative approach to defining position within the tidal zone. In: *Sedimentation on the Modern Carbonate Tidal Flats on Northwest Andros Island, Bahamas* (Ed. L.A. Hardie), pp. 7–11. The Johns Hopkins University Press, Baltimore, MD.

Glennie, K.W., Boeuf, M.G.A., Hughes Clarke, M.W., Moody-Stuart, M., Pilaar, W.F.H., Reinhardt, B.M. (1974) Geology of the Oman Mountains. *Verhandelingen van het nederlands geologisch mijnbouwkundig Genootenschap*, **31,** 423.

Gomez, J.J. and **Fernandez-Lopez, S.** (1994) Condensation processes in shallow platforms. *Sed. Geol.*, **92,** 147–159.

Handford, C.R. and **Loucks, R.G.** (1993) Carbonate depositional sequences and systems tracts – response of carbonate platforms to relative sea-level changes. *AAPG Mem.*, **57,** 3–42.

Hardie, L.A. and **Shinn, E.A.** (1986) Carbonate depositional environments, modern and ancient. Part 3 – Tidal flats. *Colorado School Mines Quart.*, **81,** 1–74.

Heim, A. (1924) Über submarine Denudation und chemische Sedimente. *Geologische Rundschau*, **15,** 1–47.

Hillgärtner, H. (1998) Discontinuity surfaces on a shallow-marine carbonate platform (Berriasian, Valanginian, France and Switzerland). *J. Sed. Res.*, **68,** 1093–1108.

Hughes, G.W. (2000) Bioecostratigraphy of the Shu'aiba Formation, Shaybah field, Saudi Arabia. *GeoArabia*, **5,** 545–578.

Immenhauser, A. and **Scott, R.W.** (2002) An estimate of Albian sea-level amplitudes and its implication for the duration of stratigraphic hiatuses. *Sed. Geol.*, **152,** 19–28.

Immenhauser, A., Creusen, A., Esteban, M. and **Vonhof, H.B.** (2000) Recognition and interpretation of polygenic discontinuity surfaces in the Middle Cretaceous Shu'aiba, Nahr Umr and Natih Formations of Northern Oman. *GeoArabia*, **5,** 299–322.

Immenhauser, A., Kenter, J.A.M., Ganssen, G., Bahamonde, J.R., Van Vliet, A. and **Saher, M.H.** (2002) Origin and significance of isotope shifts in Pennsylvanian carbonates (Asturias, NW Spain). *J. Sed. Res.*, **72,** 82–94.

Immenhauser, A., Della Porta, G., Kenter, J.A.M. and **Bahamonde, J.R.** (2003) An alternative model for positive shifts in shallow-marine carbonate $\delta^{13}C$ and $\delta^{18}O$. *Sedimentology*, **50,** 953–960.

Immenhauser, A., Hillgärtner, H., Sattler, U., Bertotti, G., Van der Kooij, B., Van Bentum, E., Van Koppen, J., Verwer, K., Immenhauser-Potthast, I., Schoepfer, P., Vahrenkamp, V., Hoogerduijn-Strating, E., Peters, J., Homewood, P., Droste, H.J., Swinkels, W., Steuber, T., Masse, J.P. and **Al Maskery, S.A.J.** (2004) The Barremian-Lower Aptian Qishn Formation (Huqf Area, Oman): an outcrop analogue for Kharaib/Shuaiba Subsurface Reservoirs. *GeoArabia*, **9,** 153–194.

Immenhauser, A., Hillgärtner, H. and **Van Bentum, E.** (2005) Microbial-foraminiferal episodes in the Early Aptian of the southern Tethyan margin: ecological significance and possible relation to oceanic anoxic sub-event 1a. *Sedimentology*, **52,** 77–99.

Jenkyns, H.C. and **Wilson, O.A.** (1999) Stratigraphy, paleoceanography and evolution of Cretaceous Pacific Guyots: Relicts from a Greenhouse world. *Am. J. Sci.*, **299,** 341–392.

Joachimski, M. (1994) Subaerial exposure and deposition of shallowing upward sequences: evidence from stable isotope of Purbeckian peritidal carbonates (basal Cretaceous), Swiss and French Jura Mountains. *Sedimentology*, **41,** 805–824.

Kauffman, E.G., Elder, W.P. and **Sageman, B.B.** (1991) High-Resolution Correlation: a New Tool in Chronostratigraphy. In: *Cycles and Events in Stratigraphy* (Eds G. Einsele, W. Ricken and A. Seilacher), pp. 795–820. Springer, Berlin.

Kendall, C.G. and **Warren, J.** (1987) A review of the origin and setting of tepees and their associated fabrics. *Sedimentology*, **34,** 1007–1028.

Klappa, C.F. (1980) Rhizoliths in terrestrial carbonates: classification, recognition, genesis and significance. *Sedimentology*, **27,** 613–629.

Le Metour, J., Michel, J.C., Bechennec, F., Platel, J.P. and **Roger, J.** (1995) *Geology and Mineral Wealth of the Sultanate of Oman*. Muscat, Ministry of Petroleum and Minerals, Directorate General of Minerals, Sultanate of Oman and Bureau de Recherches et Minieres, France, Muscat, 285 pp.

Lohman, K.C. (1988) Geochemical Patterns of meteoric diagenetic systems and their application to studies of paleokarst. In: *Paleokarst* (Eds N.P. James and P.W. Choquette), pp. 58–80, Springer, Berlin.

Loosveld, R.J.H., Bell, A. and **Terken, J.J.M.** (1996) The tectonic evolution of interior Oman. *GeoArabia*, **1,** 28–51.

Marshall, D., Jr and **Ashton, M.** (1980) Isotopic and trace element evidence for submarine lithification of hardgrounds in the Jurassic of eastern England. *Sedimentology*, **27,** 271–289.

Menegatti, A.P., Weissert, H., Brown, R.S., Tyson, R.V., Farrimond, P.A.S., Caron, M. (1998) High-resolution $\delta^{13}C$ stratigraphy through the early Aptian ''Livello Selli'' of the Alpine Tethys. *Paleoceanography*, **13,** 530–545.

Mitchum, R.M., Vail, P.R. and **Thompson, S.** (1977) Seismic stratigraphy and global changes of sea level, Part two: the depositional sequence as a basic unit for stratigraphic analysis. In: *Seismic Stratigraphy — Applications to Hydrocarbon Exploration* (Ed. C.E. Payton), *AAPG Mem.*, **26,** 53–62.

Montenat, C., Barrier, P., Soudet, H.J. (2003) Aptian faulting in the Haushi-Huqf (Oman) and the tectonic evolution of the southeast Arabian platform-margin. *GeoArabia*, **8,** 643–662.

Norris, R.D., Kroon, D., Huber, B.T., Erbacher, J. (2001) Cretaceous-Paleogene ocean and climate change in the subtropical North Atlantic. In: *Western North Atlantic Paleogene and Cretaceous Paleoceanography* (Eds D. Kroon, R.D. Norris and A. Klaus), *Geol. Soc. London Spec. Publ.*, **183,** 1–22.

Patterson, W.P. and **Walter, L.M.** (1994) Depletion of ^{13}C in seawater ΣCO_2 on modern carbonate platforms: significance for the carbon isotopic record of carbonates. *Geology*, **22,** 885–888.

Pearson, P.N., Ditchfield, P.W., Singano, J., Hracourt-Brown, K.G., Nicholas, C.J., Olsson, R.K., Shackleton, N.J., Hall,

M.A. (2001) Warm tropical sea surface temperatures in the Late Cretaceous and Eocene epochs. *Nature*, **413,** 481–487.

Rankey, R. (2002) Spatial patterns of sediment accumulation on a Holocene carbonate tidal flat, northwest Andros Island, Bahamas. *J. Sed. Res.*, **72,** 591–601.

Read, J.F. and **Horbury, A.D.** (1994) Eustatic and tectonic controls on porosity evolution beneath sequence-bounding unconformities and parasequence disconformities on Carbonate Platforms. In: *Diagenesis and Basin Development* (Eds A.D. Horbury and A.G. Robinson), *AAPG Stud. Geol.*, **36,** 155–197.

Riding, R. and **Wright, V.P.** (1981) Paleosols and tidal-flat/lagoon sequences on a Carboniferous carbonate shelf: sedimentary associations of triple disconformities. *J. Sed. Petrol.*, **51,** 1323–1339.

Ries, A.C. and **Shackleton, R.M.** (1990) Stuctures in the Huqf-Haushi Uplift, east Central Oman. In: *The Geology and Tectonics of the Oman Region* (Eds A.H.F. Robertson, M.P. Searle and A.C. Ries), *Geol. Soc. London, Spec. Publ.*, **49,** 653–654.

Sarg, J.F. (1988) Carbonate sequence stratigraphy. In: *Sea-level Changes: An Integral Approach* (Eds C.K. Wilgus, B.S. Hastings, C.G.St.C. Kendall, H.W. Posamentier, C.A. Ross and J.C. van Wagoner), *Soc. Econ. Paleont. Miner. Spec. Publ.*, **42,** 155–181.

Schlager, W. (1993) Accommodation and supply – a dual control on stratigraphic sequences. *Sed. Geol.*, **86,** 111–136.

Sharland, P.R., Archer, R., Casey, D.M., Davies, R.B., Hall, S.H., Heward, A.P., Horbury, A.D. and **Simmons, M.D.** (2001) *Arabian Plate Sequence Stratigraphy*. Gulf PetroLink, Bahrain, 371 pp.

Shinn, E.A. (1969) Submarine lithification of Holocene carbonate sediments in the Persian Gulf. *Sedimentology*, **12,** 109–144.

Shinn, E.A. (1983) Tidal flat environment. In: *Carbonate Depositional Environments* (Eds P.A. Scholle, D.G. Bebout and C.H. Moore), *AAPG Mem.*, **33,** 171–210.

Shinn, E.A., Ginsburg, R.N. and **Lloyd, R.M.** (1965) Recent supratidal dolomite from Andros Island, Bahamas. In: *Dolomitization and Limestone Diagenesis* (Eds L.C. Pray and R.C. Murray), *SEPM Spec. Publ.*, **13,** 112–123.

Steuber, T. (2002) Plate tectonic control on the evolution of Cretaceous platform-carbonate production. *Geology*, **30,** 259–262.

Strasser, A. (1991) Lagoonal–peritidal sequences in carbonate environments: autocyclic and allocyclic processes. In: *Cycles and Events in Stratigraphy* (Eds G. Einsele, W. Ricken and A. Seilacher), pp. 285–301. Springer, New York.

Sweeting, M. (1979) *Problems in Karst Environments*. Gebrueder Borntraeger, Stuttgart-Berlin, 106 pp.

Swift, D.J.P. (1968) Coastal erosion and transgressive stratigraphy. *J. Geol.*, **76,** 444–456.

Swift, D.J.P. (1978) Coastal sedimentation. In: *Marine Sediment Transport and Environmental Management* (Eds D.J. Stanley and D.J.P. Swift), pp. 255–311. J. Wiley and Sons, New York.

Swift, D.J.P., Parsons, B.S., Foyle, A. and **Oertel, G.F.** (2003) Between beds and sequences: stratigraphic organization at intermediate scales in the Quarternary of the Virginia coast, USA. *Sedimentology*, **50,** 81–111.

Tucker, M.E. and **Wright, P.V.** (1990) *Carbonate Sedimentology*. Blackwell Science, London, 482 pp.

Vahrenkamp, V. (1996) Carbon isotope stratigraphy of the Upper Kharaib and Shuaiba Formations: implications for the Early Cretaceous evolution of the Arabian Gulf Region. *AAPG Bull.*, **80,** 647–662.

Van Buchem, F., Pittet, B., Hillgärtner, H., Groetsch, J., Al Mansouri, A.I., Billing, I.M., Droste, H.J. and **Oterdoom, W.H.** (2002) High-resolution Sequence Stratigraphic Architecture of Barremian/Aptian Carbonate Systems in Northern Oman and the United Arab Emirates (Kharaib an Shu'aiba Formations). *GeoArabia*, **7,** 461–500.

Veizer, J., Ala, D., Azmy, K., Bruckschen, P., Buhl, D., Bruhn, F., Carden, G.A.F., Diener, A., Ebneth, S., Godderis, Y., Jasper, T., Korte, C., Pawellek, S., Podlaha, O.G. and **Strauss, H.** (1999) ^{87}Sr, $\delta^{13}C$ and $\delta^{18}O$ evolution of Phanerozoic seawater. *Chem. Geol.*, **161,** 59–88.

Wagner, P.D., Tasker, D.R. and **Wahlman, G.P.** (1995) Reservoir degradation and compartmentalization below subaerial exposure unconformities: Limestone examples from West Texas, China and Oman. In: *Unconformities and Porosity in Carbonate Strata* (Eds D.A. Budd, A.H. Saller and P.M. Harris), *AAPG Spec. Publ.*, **63,** 177–195.

Weissert, H., Lini, A., Foellmi, K.B. and **Kuhn, O.** (1998) Correlation of early Cretaceous carbon isotope stratigraphy and platform drowning events: a possible link? *Paleogeogr. Paleoecol. Paleoclimatol.*, **137,** 189–203.

Wilkinson, B.H., Diedrich, N.W. and **Drummond, C.N.** (1996) Facies successions in peritidal carbonate sequences. *J. Sed. Res.*, **66,** 1065–1078.

Wilkinson, B.H., Drummond, C.N., Rothman, E.D. and **Diedrich, N.W.** (1997) Stratal order in peritidal carbonate sequences. *J. Sed. Res.*, **67,** 1068–1082.

Wilson, M. and **Taylor, P.D.** (2001) Palaeoecology of hard substrate faunas from the Cretaceous Qahlah Formation of the Oman Mountains. *Paleontology*, **44,** 21–41.

Wright, V.P. (1994) Paleosols in shallow-marine carbonate sequences. *Earth-Sci. Rev.*, **35,** 367–395.

Manuscript received 21 August 2003; revision accepted 18 December 2004